catalysts

MDPI

Article

Plant-Based Copper Oxide Nanoparticles; Biosynthesis, Characterization, Antibacterial Activity, Tanning Wastewater Treatment, and Heavy Metals Sorption

Ahmed M. Eid [1], Amr Fouda [1,*], Saad El-Din Hassan [1,*], Mohammed F. Hamza [2,3], Nada K. Alharbi [4], Amr Elkelish [5,6], Afaf Alharthi [7] and Waheed M. Salem [8]

1 Department of Botany and Microbiology, Faculty of Science, Al-Azhar University, Nasr City, Cairo 11884, Egypt
2 School of Nuclear Science and Technology, University of South China, Hengyang 421001, China
3 Nuclear Materials Authority, P.O. Box 530, El-Maadi, Cairo 11728, Egypt
4 Department of Biology, College of Science, Princess Nourah bint Abdulrahman University, P.O. Box 84428, Riyadh 11671, Saudi Arabia
5 Biology Department, College of Science, Imam Mohammad ibn Saud Islamic University (IMSIU), P.O. Box 90950, Riyadh 11623, Saudi Arabia
6 Botany and Microbiology Department, Faculty of Science, Suez Canal University, Ismailia 41522, Egypt
7 Department of Clinical Laboratory Sciences, College of Applied Medical Sciences, Taif University, Taif 21944, Saudi Arabia
8 Medical Labs Department, Faculty of Applied Health Science Technology, Menoufia University, Shebine El-Koam 32511, Egypt
* Correspondence: amr_fh83@azhar.edu.eg (A.F.); saad_hassan@azhar.edu.eg (S.E.-D.H.)

Citation: Eid, A.M.; Fouda, A.; Hassan, S.E.-D.; Hamza, M.F.; Alharbi, N.K.; Elkelish, A.; Alharthi, A.; Salem, W.M. Plant-Based Copper Oxide Nanoparticles; Biosynthesis, Characterization, Antibacterial Activity, Tanning Wastewater Treatment, and Heavy Metals Sorption. *Catalysts* **2023**, *13*, 348. https://doi.org/10.3390/catal13020348

Academic Editors: Ciro Bustillo-Lecompte, Mehrab Mehrvar, Lesly Tejeda-Benitez and Fiderman Machuca-Martínez

Received: 11 January 2023
Revised: 27 January 2023
Accepted: 30 January 2023
Published: 3 February 2023

Abstract: Herein, the aqueous extract of *Portulaca oleracea* has been used as a safe, cheap, eco-friendly, and applicable scale-up method to bio-fabricate copper oxide nanoparticles (CuO-NPs). The character of CuO-NPs were determined using UV-vis spectroscopy, Fourier transform infrared (FT-IR), X-ray diffraction (XRD), Transmission electron microscopy (TEM), Energy dispersive X-ray(EDX), Dynamic light scattering (DLS), and zeta potential. Spherical and crystalline CuO-NPs with a size range of 5–30 nm at a maximum surface plasmon resonance of 275 nm were successfully fabricated. The main components of the green-synthesized particles were Cu and O with weight percentages of 49.92 and 28.45%, respectively. A Zeta-potential value of −24.6 mV was recorded for CuO-NPs, indicating their high stability. The plant-based CuO-NPs showed promising antimicrobial and catalytic activity in a dose-dependent manner. Results showed that the synthesized CuO-NPs had the efficacy to inhibit the growth of pathogens *Staphylococcus aureus*, *Bacillus subtilis*, *Escherichia coli*, *Pseudomonas aeruginosa*, and *Candida albicans* with low MIC values in the ranges of 6.25–25 µg/mL. The highest decolorization percentages of tanning wastewater were attained under sunlight irradiation conditions at a concentration of 2.0 mg/mL after 200 min with percentages of 88.6 ± 1.5% compared to those which were recorded under dark conditions (70.3 ± 1.2%). The physicochemical parameters of tanning wastewater including total suspended solids (TSS), total dissolved solids (TDS), chemical oxygen demand (COD), biological oxygen demand (BOD), and conductivity under optimum conditions were significantly decreased with percentages of 95.2, 86.7, 91.4, 87.2, and 97.2%, respectively. Interestingly, the heavy metals including cobalt (Co), lead (Pb), nickel (Ni), cadmium (Cd), and chromium (Cr (VI)) decreased with percentages of 73.2, 80.8, 72.4, 64.4, and 91.4%, respectively, after treatment of tanning wastewater with CuO-NPs under optimum conditions. Overall, the plant-synthesized CuO-NPs that have antimicrobial and catalytic activities are considered a promising nano-catalyst and environmentally beneficial to wastewater treatment.

Keywords: green synthesis; pathogenic microbes; leather effluent; heavy metals

1. Introduction

Widespread antibiotic-resistant bacteria cause several thousand deaths annually and are caused by antibiotics overuse and the transmission of antibiotic-resistant genes between different types of bacteria [1]. Therefore, efforts have focused on developing active compounds with multifunctional properties to control multi-drug resistant microbes. In addition, environmental pollution with industrial effluents such as those produced by the leather industry and heavy metals have serious negative impacts on humans, plants, animals, and other ecosystem components [2]. Remediation of the polluted sites from hazardous pollutants through simple, rapid, economical, and environmentally safe methods, such as the green synthesis of nanoparticles derived from plants extracts is urgently required [3,4]. Nanoparticles are characterized by their small sizes (1–100 nm), which give them a high surface area-to-volume ratio, along with their reactivity, solubility, strength, and mobility, as well as unique interface effects and quantum properties; this distinguish them from the bulk of materials. The innovative physical and chemical properties of nanomaterials potentially provide uses in several environmental, engineering, biological, and medical applications [5–7]. Copper and their oxide nanoparticles (CuO-NPs/Cu-NPs) have attracted more attention as one of the most important metal nanoparticles because of their beneficial properties to plants in terms of defense, growth, and nutrition. These nanoparticles have also been used in nanomedicine due to their antifungal, antiviral, and antibacterial properties, in addition to their impact on cancer therapy. Moreover, they can be used as catalysts for environmental clean-up of pollutants [8,9].

Conventional synthesis of nanoparticles using chemical and physical methods such as chemical reduction, hydrothermal, and sol-gel methods is considered harmful to the environment due to their toxic chemical products as well as their cost. Therefore, bio-fabrication of nanoparticles using algae, microorganisms, and plant extracts has attracted attention for being an environmentally safe choice. However, green-synthesized nanomaterials using plant extracts is the best biological option for their ease of handling, availability, low cost, and compatibility with medical applications such as cancer treatment, antifungal and antibacterial properties, and drug delivery, besides their use as insecticides [10].

Portulaca olracea (purslane) is an annual plant that belongs to the *Portulacaceae* family. It is a highly nutritious herb that is rich in several important phytochemicals such as sterols, flavonoids, polysaccharides, fatty acids (high omega-3 content), alkaloids, terpenoids, vitamins, proteins, minerals, calcium, magnesium, ascorbic acid, and tocopherols. Purslane has been used in folk medicine and has been shown to possess many medicinal properties such as antioxidant, neuroprotective, antidiabetic, antiulcerogenic, anticancer, anti-inflammatory, antioxidant, and antimicrobial activities. Moreover, it can be used for improving lipid profiling, glucose control, and blood pressure in adults [11]. Due to the richness of purslane with many phytochemicals, purslane extracts have been used in the biosynthesis of various nanoparticles such as selenium, silver, and zinc oxide [4,12]. However, the literature is sparse on the use of purslane aqueous extract to fabricate CuO-NPs for biomedicals and biotechnological applications. Recently, the aqueous leaf extract of *portulaca oleracea* was employed as a functional biological reductant for the synthesis of tinny copper nanocrystals (2.4–8.3 nm diameters) [13]. In addition, the aqueous extract of purslane leaves have been used to biosynthesis CuO-NPs in order to produce promising anti-inflammatory and antioxidant applications [14].

Among the unique physical, chemical, and optical properties of nanoparticles, the large surface area is the most important advantage as it provides active adsorption sites and thus can be adapted for effluent treatment. Moreover, some nanoparticles can be used sustainably due to their reusability. In addition, the use of nanotechnology for wastewater treatment does not require infrastructure, is applicable, and cost-effective. Thus, the potential use of nanotechnology for wastewater treatment is beneficial in developing countries [15]. Tanneries discharge large quantities of polluted water with dyes, tannins, solvents, alkalis, acids, chlorides, chromium salts, sulfides, and proteins, causing serious environmental damage and posing a major threat to human health [16]. Recently, nan-

otechnology has been used to improve the quality of wastewater and rid it of organic and inorganic pollutants that are difficult to remove with conventional methods. In this context, photocatalysts, nano-adsorbents, nano-films, and nano-metals were used, especially nano-copper oxide which was 94.5% effective for removing chemical oxygen demand from contaminated water in a time-dependent manner under standard conditions [17]. Moreover, bio-generated CuO-NPs were efficiently used for bioremediation of textile wastewater with 90% dye removal and elimination of 30, 55, and 93% nickel (Ni), chromium (Cr), and lead (Pb), respectively [18]. It has been shown that several parameters govern the use of CuO as one of the commonly used nanoparticles to remove Ni, Pb, and cadmium (Cd) from polluted water, such as contact time, nano-sorbent dose, pH, and metal ion concentrations [19]. Similarly, myco-synthesized MgO-NPs have shown outstanding efficacy in the treatment of tanning effluents, recording more than 95% color removal capacity, about 97% removal of chromium ions, and a reduction in the conductivity and chemical properties of the treated water, including total suspended solids (TSS), total dissolved solids (TDS), chemical oxygen demand (COD), and biological oxygen demand (BOD) [20]. Therefore, the use of green-synthesized materials is safe, eco-friendly, and has biocompatibility with the treatment of industrial wastewater and removal of heavy metals. These are considered the main challenges to overcome the disadvantages of the chemical materials used. The importance of these new materials is increased when they have antibacterial and antifungal activity. To the best of our knowledge, this is the first report about the biotreatment of tanning wastewater using CuO-NPs fabricated using purslane aqueous extract.

Hence, the novelty of the current study can be summarized as the use of green-synthesized NPs fabricated using Egyptian purslane extract in biomedical biotechnological sectors as antimicrobial agents and environmental catalysts for treatment of tanning effluents and heavy metal sorption. The green-synthesized CuO-NPs were characterized using UV-vis spectroscopy, Fourier transform infrared (FT-IR), X-ray diffraction (XRD), Transmission electron microscopy (TEM), Energy dispersive X-ray (EDX), Dynamic light scattering (DLS), and zeta potential. The antimicrobial activity of biogenic CuO-NPs against varied bacterial and fungal pathogens including *Bacillus subtilis*, *Staphylococcus aureus*, *Escherichia coli*, *Pseudomonas aeruginosa,* and *Candida albicans* was evaluated. Moreover, the effectiveness of CuO as a nano-sorbent in the treatment of tannery effluents was evaluated for decolorization and to improve the physicochemical parameters, as well as to remediate polluted water with heavy metals.

2. Results and Discussion

2.1. Green Synthesis of CuO-NPs

P. oleracea-mediated green synthesis of CuO-NPs has various advantages over chemical, physical, and other biological approaches not only due to it is eco-friendly and nontoxic method, but also economically, by avoiding unfavorable and expensive treatments such as temperature and pH, as with chemical and physical approaches. In addition, the worldwide availability of this plant grants its use as a suitable candidate for large scale-up of the industrial sector and to avoid the pathogenicity of microorganisms-mediated biosynthesis [21,22]. This plant has diverse active compounds such as alkaloids, flavonoids, fatty acids, polysaccharides, proteins, sterols, vitamins, terpenoids, and minerals [11]. Herein, the green synthesis of CuO-NPs depends on the presence of these active metabolites in plant aqueous extract which is responsible for the reduction of Cu^{2+} to Cu^{0} followed by capping and stabilizing of the final product [4]. In the current study, the formation of a greenish color after mixing the aqueous extract with $Cu(CH_3COO)_2.H_2O$ and adjusting the pH at 8 indicates the successful formation of CuO-NPs. In contrast, the plant aqueous extract in the absence of metal precursor under the same conditions did not exhibit any color change. Similarly, the greenish color was formed after mixing copper sulfate with leaf aqueous extract of *Enicostemma axillare* [23]. The visual observation of aqueous extract after mixing with a metal precursor is the first sign for biosynthesis of CuO-NPs. The color

change from colorless to greenish could be due to the vibration and resonance of charged particles on the NPs surface as reported previously [24].

2.2. Characterization

2.2.1. Morphological Characterization (TEM, SEM, EDX)

The morphological characteristics including sizes, shapes, aggregations, and elementary mapping of green-synthesized CuO-NPs are crucial parameters affecting their bioactivities. TEM, SEM, and EDX analyses are useful techniques for investigating these parameters. As shown, the *P. oleracea*-based CuO-NPs have a spherical shape, well-arranged, without any aggregation or agglomeration. The particle size of biosynthesized CuO-NPs was in the range of 5–30 nm with average sizes of 22 nm (Figure 1A). In a similar study, the average particle size of the spherical shape of CuO-NPs fabricated using an aqueous extract of *Annona muricata* L was in the range of 16–31 nm [25]. Moreover, the extract of pumpkin seed showed high efficacy to fabricate circular CuO-NPs with an average particle size of 20 nm [26]. The biological activities of nanomaterials are directly correlated with sizes and shapes. For instance, the cytotoxic efficacy of CuO-NPs varied based on sizes between 4 nm and 24 nm. It has been reported that the CuO-NPs with sizes of 24 nm were highly toxic to adenocarcinoma cells A549 compared to size 4 nm, despite the smaller sizes having the efficacy to dissolute toxic ions (Cu^{2+}) faster than large sizes [27]. Interestingly, the antibacterial activity of the rods and platelets shapes of CuO-NPs fabricated using aqueous extract of *Aloe vera* against *E. coli* and *Staphylococcus aureus* was more effective compared to spherical shapes [28]. Increased surface energy and surface-active sites of different structural morphologies may explain the variation in activity [29].

Moreover, the topographical and morphological properties of plant-based CuO-NPs were investigated with SEM analysis (Figure 1B). As shown, the smooth surface and spherical shape of CuO-NPs were arranged without aggregation. Similarly, the spherical shape of synthesized CuO-NPs using extracts of mint leaves or orange peel was detected with SEM analysis [19]. Some aggregations in SEM images have been due to coating agents from plant extracts which may increase their size obtained under SEM compared to those obtained with TEM analysis. Interestingly, the chemical compositions of green-synthesized CuO-NPs were detected with EDX analysis as shown in Figure 1C. The EDX spectrum confirmed that the main components of the biosynthesized sample were Cu and O. The presence of absorption peak at a bending energy of 0.5 Kev refers to the O ion, whereas the peaks at bending energies of 1.0, 8.0, and 9.0 KeV correspond to Cu atoms. The quantitative analysis of atoms in the synthesized sample have shown that the weight percentages of Cu and O were 49.92 and 28.45%, whereas the atomic percentages were 39.47 and 31.11%, respectively (Figure 1C). The C peak was observed in the sample with wight and atomic percentages of 21.63 and 29.42%, respectively. This peak can be attributed to the scattering of metabolites from plant aqueous extract that coated the surface of CuO-NPs [19]. In a similar study, The EDX spectrum of CuO-NPs fabricated using seeds aqueous extract of *Salvia hispanica* showed peaks of O at a bending energy of 0.5 KeV and Cu at 1.0, 8.0, and 9.0 KeV with weight percentages of 20.1 and 79.9%, respectively [30]. The EDX analysis of CuO-NPs synthesized using leaf aqueous extract of *Azadirachta indica* showed the presence of Cu and O atoms with weight percentages of 65.33 and 34.67%, respectively [31]. The absence of other elements in the EDX analysis indicates the purity of the synthesized sample, as verified with XRD analysis. Ssekatawa et al. reported that the main components of CuO-NPs fabricated using aqueous extract of *Camellia sinensis* and *Prunus africana* were Cu and O in addition to the other peaks which referred to the presence of potassium, nitrogen, magnesium, phosphorus, and manganese [32].

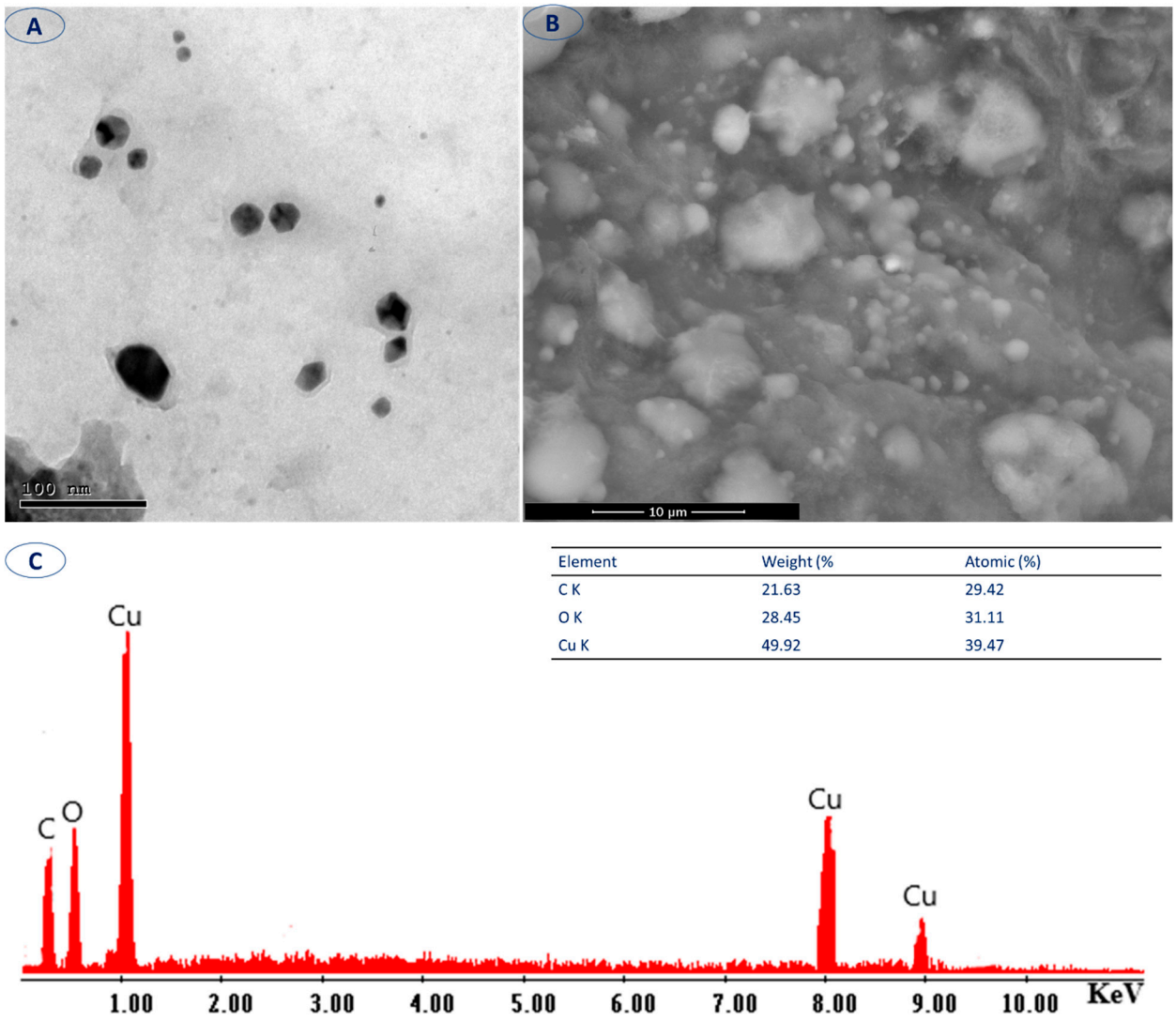

Figure 1. Characterization of CuO-NPs fabricated using aqueous extract of *P. oleracea* using transmission electron microscopy (**A**), scanning electron microscopy (**B**), and energy dispersive X-ray (**C**).

2.2.2. X-ray Diffraction

The phase structure of plant-based CuO-NPs was detected with XRD analysis which showed strong twelve diffraction peaks. Typically, Bragg's diffraction peaks were observed at 2θ values of 33.1°, 35.8°, 38.9°, 49.2°, 53.7°, 58.4°, 61.7°, 66.5°, 68.2°, 72.5°, and 75.3° that matched planes of (110), (-111), (111), (-202), (020), (202), (-113), (-311), (220), (311), and (-222), respectively (Figure 2). The obtained XRD spectrum affirmed that the plant-synthesized CuO-NPs were face-centered cubic structures with crystalline nature according to the Joint Committee on Powder Diffraction (JCPD) standard with the file number 80-1268 [33]. The observed peak at 2θ values in the range of 35–39° indicates the formation of CuO-NPs as reported previously [34]. The absence of additional peaks in the XRD pattern confirmed the high purity of biosynthesized CuO-NPs, compatible with EDX analysis. The obtained data were compatible with various literature on green-synthesized CuO-NPs [23,32,35]. Ahmed et al. reported that the sharp and well-defined Bragg's peaks in the XRD pattern indicate the successful formation of a crystallographic structure with sizes $\leq$ 100 nm [36].

The crystallite size of biosynthesized CuO-NPs can be measured via the XRD pattern by using Debye–Scherrer's equation. In the current study, the average crystallite size was 21 nm. Similarly, the average crystallite size of CuO-NPs synthesized by harnessing

plant metabolites of *Azadirachta indica* was close to 7 nm [31]. On the other hand, the mean average crystallite sizes of CuO-NPs obtained using XRD analysis were 43 nm and 38 nm for those synthesized using plant extract of *Prunus Africana* and *Camellia sinensis*, respectively [32].

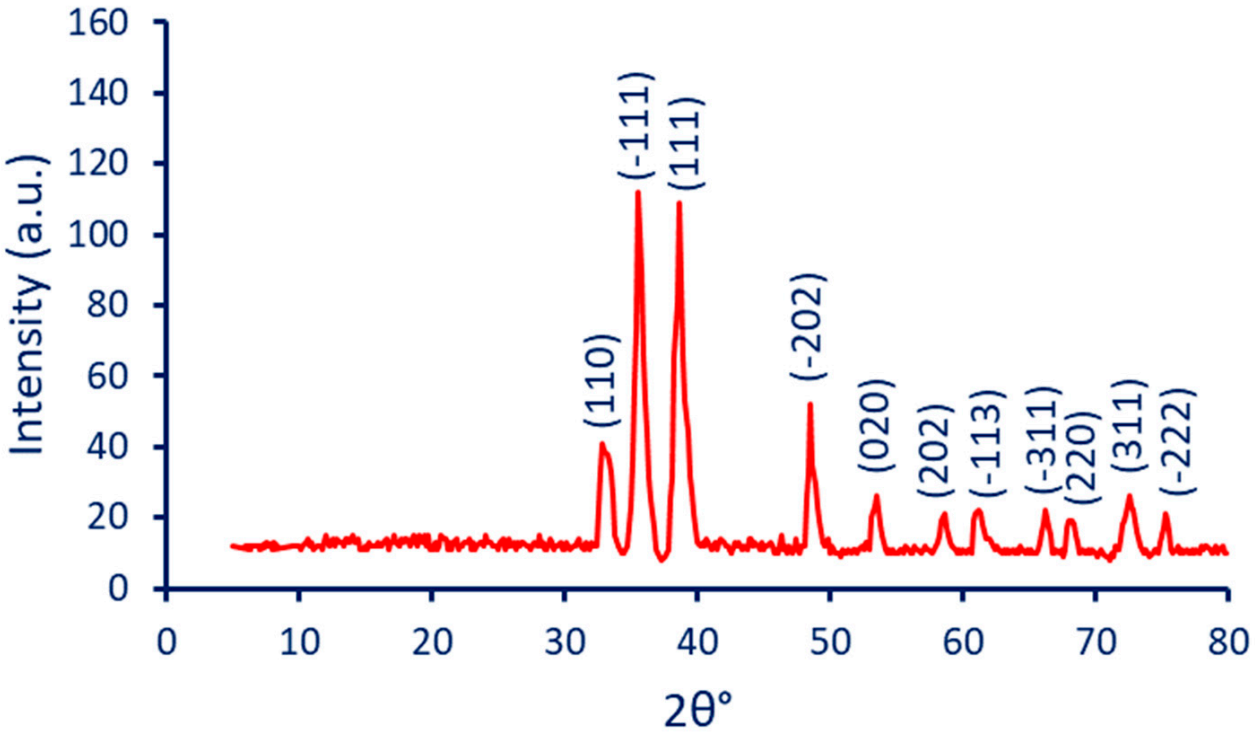

Figure 2. X-ray diffraction pattern of CuO-NPs synthesized using aqueous extract of *P. oleracea*.

2.2.3. Fourier Transform Infrared (FT-IR)

The functional groups present in plant aqueous extract and their role in the reduction of metal precursors, converting to nanoscale, followed by capping and stabilizing of final products, are investigated using FT-IR analysis. The aqueous extract contains eight peaks at wavenumbers 3400, 2077, 1633, 1404, 1310, 1100, 1012, and 700 cm^{-1} (Figure 3). These peaks are shifted and change their intensity after the formation of CuO-NPs. The broad, strong peak at 3400 cm^{-1} signified the stretching of the hydroxyl group (OH) which overlapped with the NH stretching of primary amines [37,38]. This peak was shifted to a wavenumber of 3420 cm^{-1} after CuO-NPs synthesis (Figure 3). The weak peaks at 2960 and 2850 cm^{-1} in the final product could be related to the C–H of aliphatic hydrocarbons [39]. The strong peak at 2077 cm^{-1} related to the aromatic compounds in plant extract, overlapped with ν(C-O) [40]. The appearance of new peaks in the final product in the ranges of 2150–2500 cm^{-1} may be related to the C≡C of alkynes, C≡N stretch of nitriles, or adsorption of CO_2 on the surface of CuO-NPs [41–43]. The strong peak at 1633 cm^{-1} in the plant extract related to the primary and secondary amides of proteins and the C=O stretch of polysaccharide moieties [4]. This peak was shifted to 1570 cm^{-1} after the fabrication of CuO-NPs which correspond to C=O and C=N for carboxylic and carbonyl groups, respectively, or I and II amides [44,45]. The medium peaks at the range of 1300–1404 cm^{-1} in plant extract correspond to the bending of O–H groups of alcohol [41], which shifted to 1410 cm^{-1} after the fabrication of CuO-NPs. Other peaks in plant aqueous extract such as 1100 cm^{-1} related to the ν(C–O–C) carbohydrate overlapped C–O stretching [46,47], 1012 cm^{-1} signify stretching of C–N [48], and 700 cm^{-1} corresponds to the bending of C-H out of plane [49]. These peaks were shifted to 1134, 1099, and 1016 cm^{-1} in the green-synthesized CuO-NPs. The presence of peaks in the ranges of 800–900 cm^{-1} was attributed to the aromatic C–H in the plan bend [50,51]. The successful formation of Cu–O was confirmed by the presence

of peaks in the wavenumber ranges of 500–700 cm^{-1} as reported previously [3,30,32]. The FT-IR spectrum confirmed the role of different functional groups in plant aqueous extract such as proteins, polysaccharides, I, and II amides in the reduction of $Cu(CH_3COO)_2.H_2O$ to form CuO-NPs followed by capping of the surface of the final product to increase its stability.

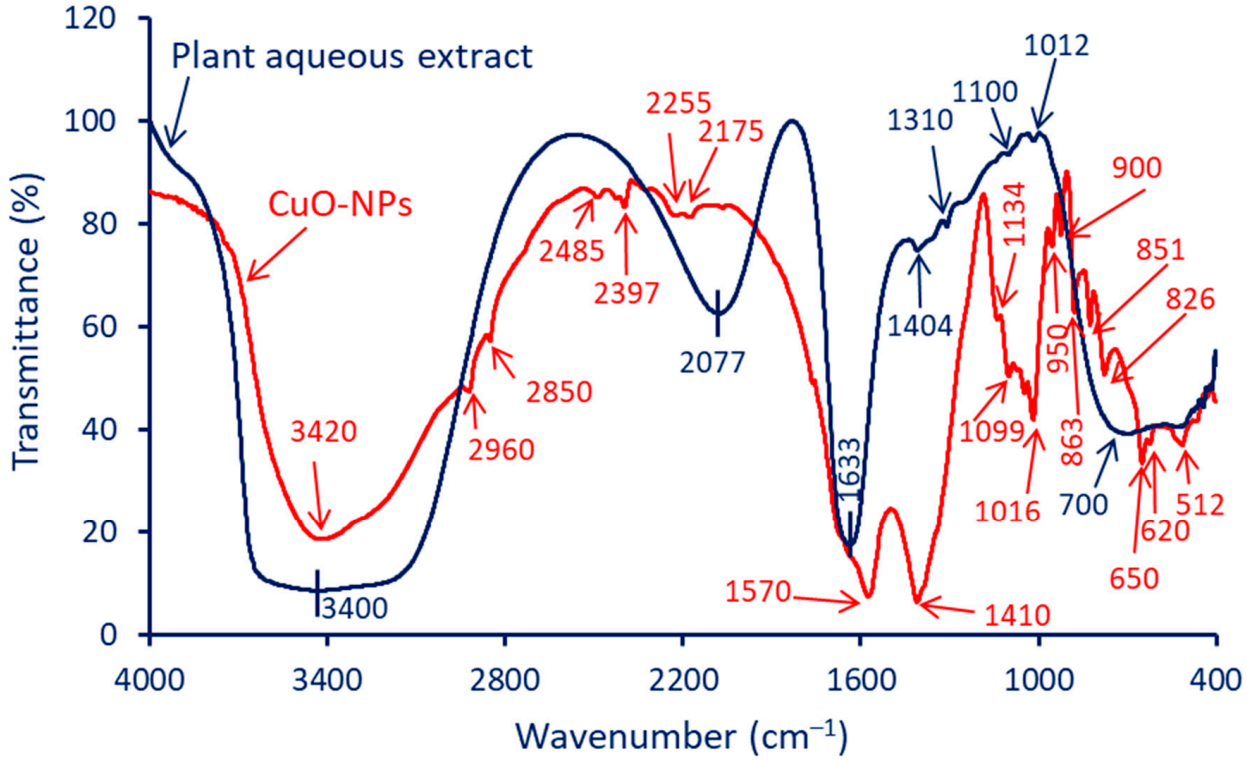

Figure 3. FT-IR of plant aqueous extract versus the biosynthesized CuO-NPs showing the presence of various functional groups.

2.2.4. UV-Vis Spectroscopy

The change of color due to NP formation is measured using UV-Vis spectroscopy to detect the maximum surface plasmon resonance (SPR). This maximum peak is obtained as a result of the repulsion of free electrons on the NPs surface, with light intensity at a specific wavelength [8]. In the current study, the maximum peak was observed at a wavelength of 275 nm which corresponds to the maximum SPR of CuO-NPs (Figure 4A). Compatible with the obtained result, the maximum SPR of CuO-NPs fabricated using leaf aqueous extract of *Vitex negundo* was observed at 274 nm [9]. Moreover, the SPR peak of CuO-NPs synthesized using the alcoholic extract of *Phoenix dactylifera* was localized at 275 nm [52]. Several factors such as crystalline nature, crystallite size, shape, the concentration of the metal precursor, and aggregations can affect the SPR peak of NPs [53]. The presence of a single SPR peak in the UV chart at a wavelength below 300 nm gives a further indication of the shape and size of CuO-NPs which may be spherical with a smaller size [54].

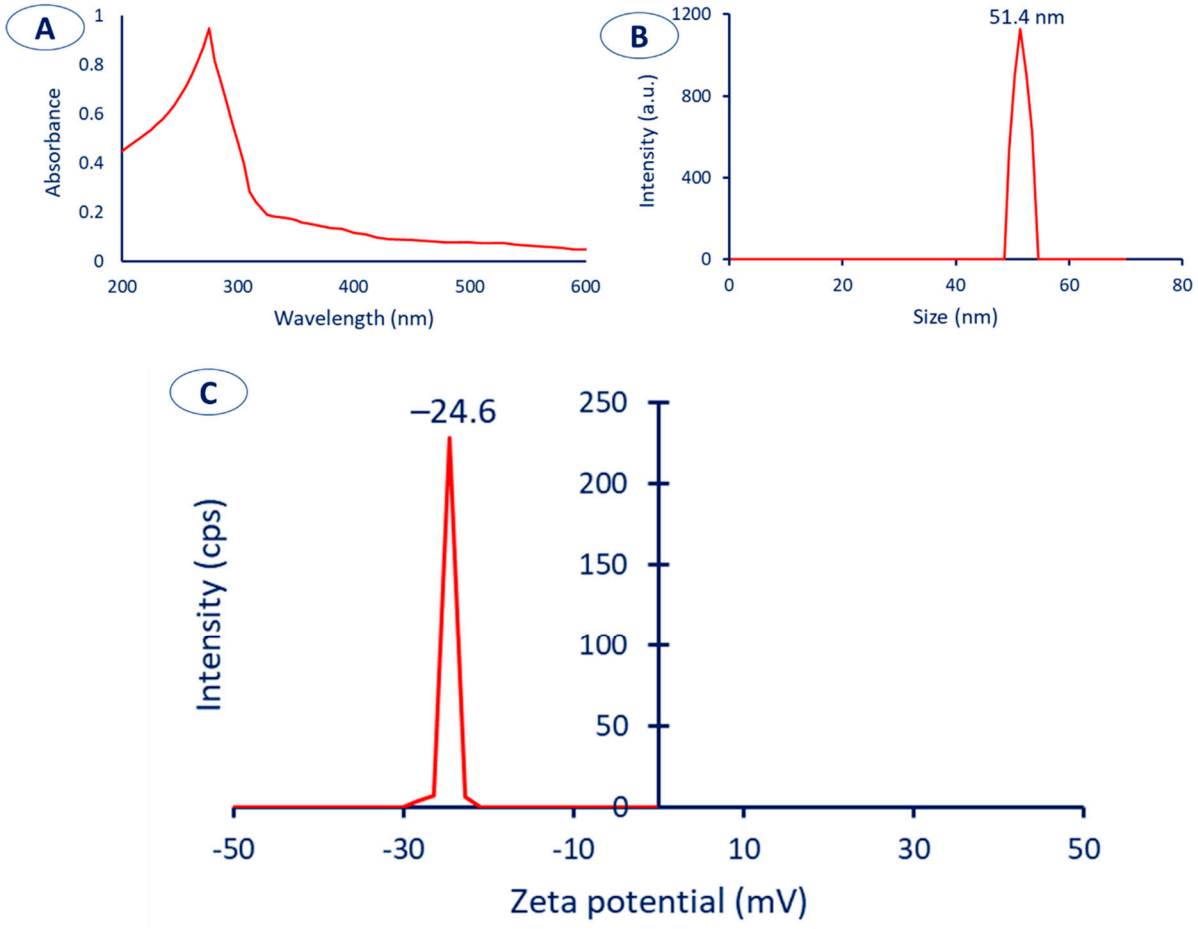

Figure 4. Characterization of plant-based CuO-NPs using UV-Vis spectroscopy (**A**), dynamic light scattering (**B**), and zeta potential (**C**) analysis.

2.2.5. Dynamic Light Scattering (DLS) and Electrokinetic Potential (pH_{PZC})

The size, size distribution, and hydrodynamic residue of CuO-NPs fabricated using the aqueous extract of *P. oleracea* were detected using dynamic or diffraction light scattering. As seen, the average particle size of green-synthesized CuO-NPs was 51.4 nm according to the graph of the size distribution (Figure 4B). As shown, the obtained size of plant-based CuO-NPs using DLS is bigger than the sizes observed with TEM and XRD. This finding could be related to the measurement method, which in TEM measures the size of dry (solid) particles whereas DLS is conducted using an aqueous solution and hence detects the hydrodynamic diameter (hydrated state) [23,55]. Moreover, the average particle size using DLS analysis is affected by several factors such as homogeneity percentages (the sizes increased with the non-homogenous distribution of CuO-NPs in the solution) and plant metabolites that coated the NPs surface (coating agent), which interfere with the calculation [56]. In a similar study, the sizes of CuO-NPs obtained using the leaf aqueous extract of *Enicostemma axillare* were 30 nm, 6.4 nm, 22.9 nm, and 470 nm according to SEM, TEM, XRD, and DLS analyses, respectively [23]. The average sizes of CuO-NPs fabricated using the aqueous extract of *Camellia sinensis* and *Prunus Africana* were (38, 6, and 61 nm) and (43, 8, and 68 nm) based on XRD, SEM, and DLS analyses, respectively [32].

As mentioned, the sizes obtained with DLS were affected by the homogeneity percentages of the solution; it is therefore essential to measure this homogeneity accordingly to the meaning of the polydispersity index (PDI). The homogeneity of the NPs in the colloidal solution increased when the PDI value was less than 0.4 and decreased at a value greater than 0.4. The colloidal solution was considered heterogenous (non-similar distribution) if the PDI value was greater than 1.0 [57]. In the current study, the PDI value of plant-

based CuO-NPs was 0.23, meaning the distribution of NPs in the colloidal solution was homogenous or similar.

The stability of green-synthesized CuO-NPs was investigated using electrokinetic or zeta potential. In this analysis, the synthesized NPs move in the colloidal solution after being subjected to an electric field. The stability based on electrokinetic potential is classified as highly unstable when zeta values are in the range of ±0–10 mV, relatively stable at zeta values of ±10–20 mV, moderately stable at values in the ranges of ±20–30 mV, and highly stable when zeta values are greater than ±30 mV [58]. In the current study, the zeta value of biosynthesized CuO-NPs was −24.6 mV (Figure 4C), indicating the high stability of synthesized nanomaterials. The electrokinetic scanning was achieved on a wide range scale to detect the charges on the surface of NPs. Herein, the spectrum showed that all particles have a negative charge, which means that the particles will remain divergent and in a repulsion state, which reduces the agglomeration. In addition, the stability of plant-based NPs could be attributed to the capping agents (from plant extract) such as flavonoids and alkaloids which improve the electrostatic forces between particles [4].

2.3. Antimicrobial Activity

The emergence of new microbial strains that have antibiotic resistance activity threatens human and animal health and hence increases morbidity and mortality worldwide. This challenge opens a new window for the discovery of new active compounds [59]. The researchers have benefited from advances in the science of nanotechnology and unique properties of nanoparticles to develop novel substances that have biomedical and biotechnological applications. In the current study, the activity of green-synthesized CuO-NPs against various pathogenic microbes including Gram-positive bacteria (*Staphylococcus aureus* and *Bacillus subtilis*), Gram-negative bacteria (*Pseudomonas aeruginosa* and *E. coli*), and unicellular fungi (*Candida albicans*) was evaluated using agar well diffusion method. As shown, the green-synthesized CuO-NPs have antimicrobial activity against various pathogenic microbes in a concentration-dependent manner. This finding is compatible with previous studies about the antimicrobial efficacy of NPs [8,28,60]. The highest inhibition zones were recorded for maximum concentration (200 µg mL^{-1}) with diameters of 16.7 ± 0.6, 15.7 ± 0.6, 19.3 ± 0.5, 17.7 ± 1.2, and 16.3 ± 0.6 for *B. subtilis, S. aureus, P. aeruginosa, E. coli,* and *C. albicans,* respectively, compared to a bulk material (precursor), which recorded inhibition zones of 13.7 ± 0.6, 14.7 ± 0.6, 14.3 ± 0.6, 12.6 ± 0.5, and 14.7 ± 0.6 mm, respectively, for the same previous sequence of organisms (Figure 5A–E). Similarly, the maximum zone of inhibitions was recorded for the treatment of *E. coli, Klebsiella pneumoniae,* and *S. aureus with 250* µg mL^{-1} of CuO-NPs fabricated using the aqueous extract of *Camellia sinensis* and *Prunus Africana* with diameters of (27, 27, and 30 mm) and (26, 27, and 30 mm), respectively [32]. In addition, the highest antibacterial activity of rod CuO-NPs fabricated using the aqueous fruit extract of *Momordica charantia against S. aureus, S. epidermidis, Streptococcus mutans, S. pyogenes, S. viridans, B. cereus, Corynebacterium xerosis, E. coli, K. pneumonia, P. aeruginosa*, and *Proteus vulgaris* was recorded at *250* µg mL^{-1} with a diameter of inhibition zones in the range of 25–32 nm [61]. Even though copper metals (Cu^{2+}) have antibacterial properties and are approved by US-EPA (US-Environmental Protection Agency) as a safe antimicrobial agent [62], the Cu/CuO-NPs have a higher activity compared to bulk compounds [63,64].

In the current study, the antimicrobial activity was decreased by decreasing the CuO-NPs concentrations. For instance, at 50 µg mL^{-1}, the diameter of inhibition zones decreased to 12.3 ± 0.6, 11.3 ± 0.6, 14.2 ± 0.8, 12.7 ± 0.6, and 12.3 ± 0.6 mm toward *B. subtilis, S. aureus, P. aeruginosa, E. coli,* and *C. albicans,* respectively, as compared to copper acetate at the same concentration, which recorded inhibition zones of 8.7 ± 0.6, 10.3 ± 0.5, 9.7 ± 0.6, 8.3 ± 0.6, 11.3 ± 0.6 mm (Figure 5A–E).

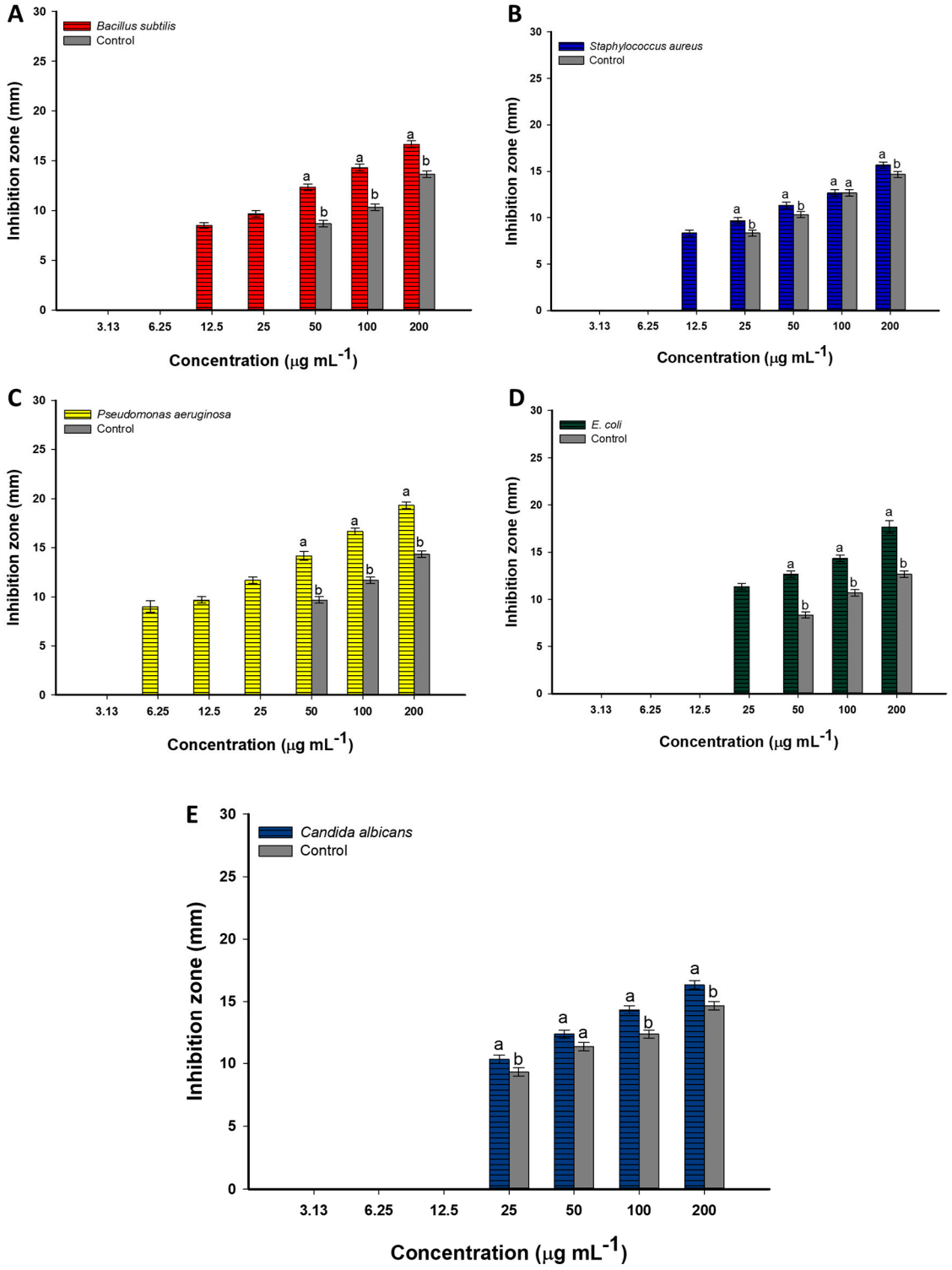

Figure 5. Antimicrobial activity of green-synthesized CuO-NPs toward Gram-positive bacteria represented by *B. subtilis* (**A**) and *S. aureus* (**B**); Gram-negative bacteria including *P. aeruginosa* (**C**) and *E. coli* (**D**), and unicellular fungi including *C. albicans* (**E**) using agar well diffusion test. Different letters on the bars indicate that the mean values are significantly different (at $p \leq 0.05$).

The minimum concentration of CuO-NPs to inhibit the growth of pathogenic microbes was defined as the minimum inhibitory concentration (MIC). It is important to detect the MIC value for each active compound before recommending incorporation in biomedical fields. Herein, the MIC value for plant-based CuO-NPs was 12.5 μg mL^{-1} for Gram-

positive bacteria, *B. subtilis*, and *S. aureus* with a zone of inhibition diameter of 8.5 ± 0.5 and 8.3 ± 0.6 mm, respectively. Whereas the MIC value for *E. coli* and unicellular fungi (*C. albicans*) was 25 12.5 μg mL^{-1} with a diameter of inhibition zones of 11.3 ± 0.6 and 10.3 ± 0.6 mm, respectively. Interestingly, the lowest MIC value (6.25 μg mL^{-1}) for CuO-NPs was recorded for *P. aeruginosa* with a zone diameter of 9.0 ± 1.0 mm (Figure 5A–E). Interestingly, the MIC for control (copper acetate) was 50 μg mL^{-1} for *B. subtilis*, *P. aeruginosa*, and *E. coli*, whereas the MIC value for *S. aureus* and *C. albicans* was 25 μg mL^{-1}. Based on MIC values, the CuO at the nanoscale structure was more active against all tested organisms compared to bulk material (copper acetate), especially at low concentrations.

Analysis of variance showed that *P. aeruginosa* was the most sensitive strain followed by *E. coli, C. albicans, B. subtilis,* and *S. aureus*. In a recent study, the MIC values of biosynthesized CuO-NPs against *E. coli, K. pneumoniae, and S. aureus* were 125, 125, and 30 μg mL^{-1} [32]. Compared to our data, it can be concluded that the CuO-NPs in the current study have high activity against prokaryotic and eukaryotic microorganisms at low concentrations. This finding could be attributed to the small sizes and spherical shape of green-synthesized CuO-NPs (5–30 nm) which enhance the entry of NPs into microbial cells. Several published studies reported that the activity of NPs increased with small sizes [27,28,65,66].

Overall, Gram-negative bacteria were more sensitive to CuO-NPs compared to Gram-positive bacteria. This phenomenon could be related to the structure of bacterial cell walls which in Gram +ve bacteria are composed of a thick layer of peptidoglycan compared to a thin layer in Gram -ve bacteria. This thick peptidoglycan layer can hinder or delay the penetration of CuO-NPs into the cells and hence delay their inhibitory action [67]. Moreover, the inhibitory effect of CuO-NPs can be related to its breakdown into the cell and liberation of toxic Cu^{2+} ions. The accumulation of these toxic ions can block the protein function via interaction with sulfhydryl groups (-SH) for some amino acids such as methionine and cysteine [54]. Moreover, as a result of the accumulation of these toxic ions, they can compete with essential ions in the cells such as Fe^{2+}, and hence prevent the efficacy of proteins from binding with the proper cofactor, leading to protein dysfunction [68]. Another inhibitory mechanism for bacterial damage via treatment with CuO-NPs is the overproduction of reactive oxygen species (ROS). These ROS such as superoxide anions, hydrogen peroxides, and hydroxyl radicals, enhance the oxidative stress to amino acids, nucleic acids, and membrane lipids, leading to enzyme deactivation and loss of the selective permeability function [69]. The activity of CuO-NPs toward *C. albicans* could be related to their efficacy for changing the sterol profile in *Candida* cell walls via inhibition of ergosterol pathway synthesis [70].

2.4. Tannery Wastewater Treatment

Discovering alternative active substances that may be used in the treatment of various industrial wastewater has been the major challenge facing various nations, particularly those that have water scarcity. During leather tanning, the excessive use of chromium ions and other organic and inorganic substances are the main sources for the toxicity of these effluents and their drainages. Ineffective treatment of these effluents is considered highly dangerous to humans, animals, plants, and the ecosystem [71]. Green nanotechnology offers a novel economic method for fabricating new active substances that are eco-friendly, with wide surface areas, and high stability, and can therefore be used to remove various contaminants [32,72]. Moreover, the use of active substances that have antimicrobial activity can help to improve the wastewater quality via killing the containing pathogenic microbes. Herein, the efficacy of biosynthesized CuO-NPs to degrade and treat tanning wastewater, as the most poisonous effluent originated from the leather industry, was investigated under darkness and in sunlit conditions. The experiment was achieved using different CuO-NPs concentrations (0.5, 1.0, 1.5, and 2.0 mg/mL) for various time intervals (20 to 200 min with intervals of 20 min). To the best of our knowledge, this is the first report for the decolorization and treatment of crude tanning wastewater using

green-synthesized CuO-NPs. Data analysis showed that the decolorization of tanning wastewater using CuO-NPs was concentration- and time-dependent. This finding could be attributed to the adsorption sites being increased at high concentration, and hence and increase in decolorization. The obtained results are compatible with published research on dye decolorization using nanomaterials [9,32,73]. At a low dose (0.5 mg/mL) under incubation conditions, the decolorization percentage was 12.9 ± 0.9% after 20 min and reached 45.9 ± 0.3% after 200 min compared to the control (1.2 ± 0.2% after 20 min and 11.9 ± 0.1% after 200 min) (Figure 6). These percentages were increased at high concentrations. For instance, the decolorization percentages were 14.0 ± 0.4 and 16.7 ± 0.4% after 20 min at 1.0 and 1.5 mg/mL, respectively, and reached 48.8 ± 0.2 and 60.7 ± 2.3% after 200 min under the same concentrations. In a similar study, the decolorization of tanning wastewater after treatment with green-synthesized MgO-NPs was attained with percentages of 16.1, 28.5, 37.8, and 53.5% after 30 min at concentrations of 0.25, 0.50, 0.75, and 1.0 µg/mL, respectively, compared to the control (1.9%). These percentages increased to 38.5, 59.4, 81.4, and 97.5% at the same previous concentrations after 180 min [20]. In a recent study, the green-synthesized γ-Fe_2O_3-NPs showed a decolorization percentage of 79.2% as a result of treatment with 1.0 mg/mL after 144 min [74]. In the current study, the maximum decolorization percentages under dark conditions were achieved after 200 min at a concentration of 2.0 mg/mL with a value of 70.3 ± 1.2% (Figure 6).

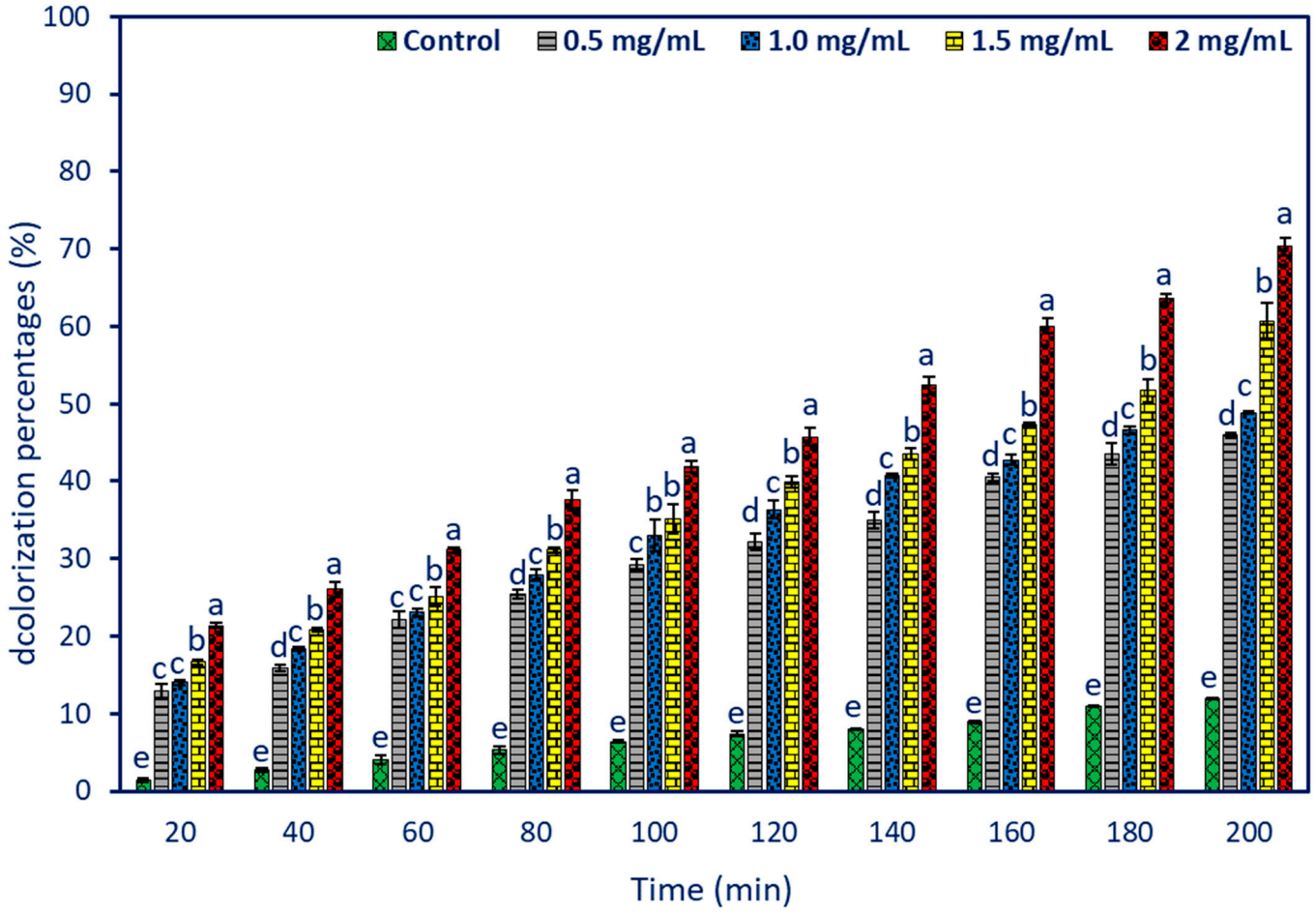

Figure 6. Decolorization percentages of tanning wastewater after treatment with different concentrations (0.5, 1, 1.5, and 2 mg/mL) of CuO-NPs at interval times (20 min to 200 min) under Dark incubation conditions. Different letters (a–e) on the bars at the same time meaning the data are significant ($p \leq 0.05$).

Interestingly, the decolorization of tanning wastewater using plant-based CuO-NPs was improved under incubation in sunlight conditions. Analysis of variance showed that the decolorization percentages were increased from 15.0 ± 0.4% after 20 min at a concentration of 0.5 mg/mL, to 59.4 ± 0.5% after 200 min at the same concentration (Figure 7). The maximum decolorization percentages under light irradiation conditions were 65.0 ± 1.1, 77.2 ± 0.4, and 88.6 ± 1.5% after 200 min at concentrations of 1.0, 1.5, and 2.0 mg/mL, respectively (Figure 7). Due to the smaller CuO-NPs sizes, the surface area was increased and hence the adsorption sites also increased [75]. Therefore, the highest decolorization percentages were attained at high CuO-NPs concentrations.

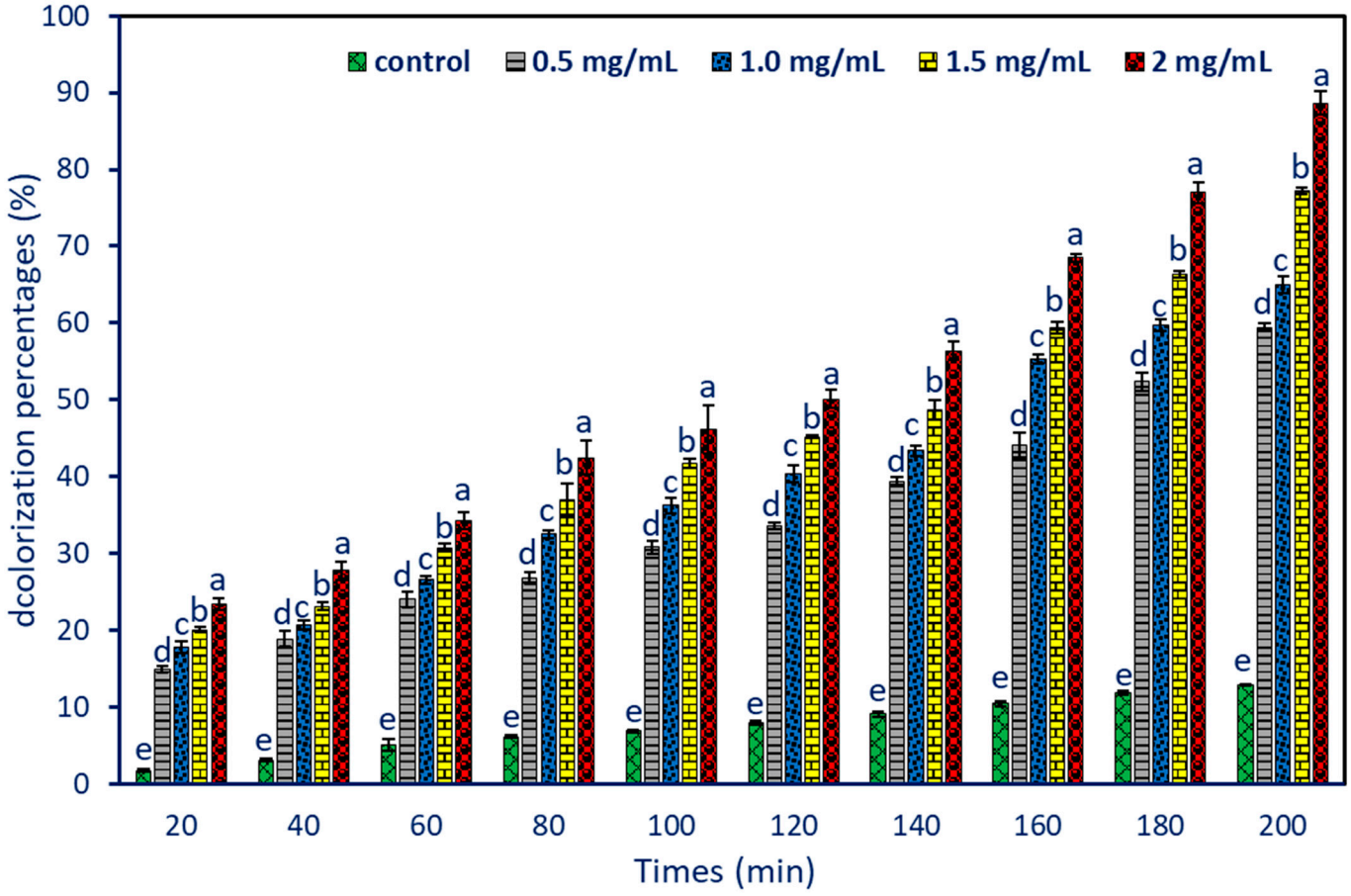

Figure 7. Decolorization percentages of tanning wastewater after treatment with different concentrations (0.5, 1, 1.5, and 2 mg/mL) of CuO-NPs at interval times (20 min to 200 min) under sunlight incubation conditions. Different letters (a–e) on the bars at the same time meaning the data are significant ($p \leq 0.05$).

The improvement of decolorization and waste treatment under sunlight conditions could be attributed to the photoexcitation of electrons on the surface of CuO-NPs, resulting in the transfer of electrons from the valence band (VB) to the conduction band (CB) ultimately leading to electron-hole pairs (e^-CB and h^+VB) production. Some free radicals such as superoxides ($^\bullet O^{2-}$) and hydrogen peroxides ($^\bullet$OOH) were formed after interacting with excited e^- in CB with O_2, whereas hydroxyl free radicals ($^\bullet$OH) were formed due to the reaction of h^+ with H_2O [51,76]. These formed free radicals reacting with contaminants and dyes in wastewater, leading to degradation into CO_2, H_2O, and other small ions (Figure 8).

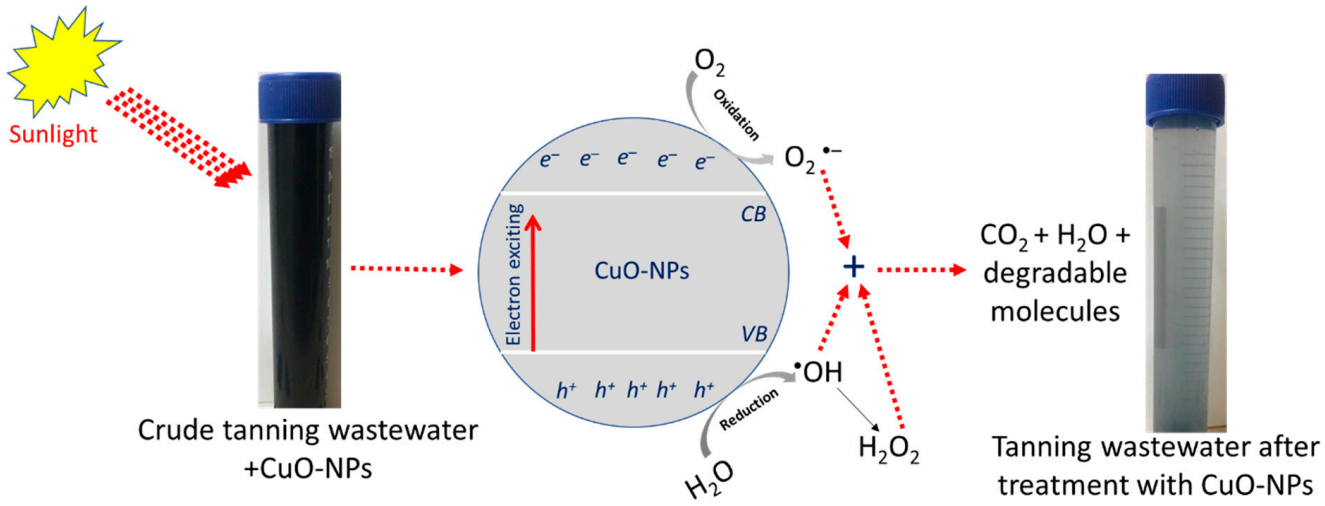

Figure 8. Photocatalytic mechanism of tanning wastewater using green-synthesized CuO-NPs.

Based on the obtained data, the physicochemical characteristics of tanning wastewater after treatment with plant-based CuO-NPs were investigated at a concentration of 2 mg/mL after 200 min under sunlight irradiation conditions, because it was recorded as the best conditions for decolorization efficacy. The wastewater parameters including pH, COD, BOD, TSS, TDS, and conductivity were assessed at optimum conditions compared to untreated wastewater. The contaminant content in tannery wastewater is broad and varies according to the size of the tannery unit, chemicals used, final products, and amount of water used during the leather tanning process [2]. Overall, the main features of tanning wastewater are high concentrations of COD, BOD, TDS, salinity, TSS, conductivity, sulfides, and heavy metals [77]. This finding could be related to the use of various chemicals during leather processing such as chlorides, calcium, bicarbonates, potassium, phosphates, sulfates, sodium, nitrates, and dissolved salts [78]. As shown, the green-synthesized CuO-NPs had the efficacy to reduce the physicochemical parameters of tanning wastewater with percentages of 91.4, 87.2, 95.2,86.7, and 97.2% for COD, BOD, TSS, TDS, and conductivity, respectively (Table 1). The alkaline conditions in crude tanning wastewater could be attributed to the excessive use of bicarbonates and carbonates during the leather tanning steps. Herein, the treatment with CuO-NPs decreased the pH values from 9.4 $\pm$ 0.2 to 6.6 $\pm$ 0.7 due to the decrease in the levels of contaminants. Therefore, it can be concluded that the green-synthesized CuO-NPs act as a promising bio-adsorbent for various contaminants in wastewater. Similarly, maghemite nanoparticles have an efficacy to decrease the COD value of tanning wastewater from 5078 to 564 mg/L with a percentage of 88.8% [79]. Zhang et al. reported that a low concentration of CuO-NPs (1 mg/L) is considered a promising concentration for decreasing the COD of wastewater versus high concentrations (30 and 50 mg/L), which can inhibit the wastewater treatment [80]. Wang et al. reported that decreasing values of COD removal during wastewater treatment at low and high concentrations of CuO-NPs were not significant. It has been reported that the removal percentage of COD using 0.1 mg/L of CuO-NPs was 91.3% whereas this value decreased to 89.5% after increasing the CuO-NPs concentration to 30 mg/L [81].

Table 1. Physicochemical parameters of tanning wastewater after treatment with CuO-NPs under optimum conditions (2.0 mg/mL, for 200 min, under sunlight irradiation conditions).

Physicochemical Parameter	Unit	Before Treatment (control)	After Treatment with 2.0 mg/mL under Sunlight Condition	Removal Percentages (%)
pH	-	9.4 ± 0.2	6.6 ± 0.7	-
COD	mg/L	791.7 ± 5.5	68.3 ± 4.1	91.4
BOD	mg/L	2434.7 ± 4.1	312.3 ± 2.5	87.2
TSS	mg/L	8907.5 ± 2.5	424.3 ± 4.2	95.2
TDS	mg/L	2702.3 ± 3.1	358.3 ± 3.1	86.7
conductivity	S/m	25792.8 ± 5.5	721.0 ± 2.6	97.2
Co	mg/L	2.55 ± 0.1	0.684 ± 0.1	73.2
Pb	mg/L	1.702 ± 0.01	0.327 ± 0.03	80.8
Ni	mg/L	2.803 ± 0.01	0.774 ± 0.05	72.4
Cd	mg/L	0.612 ± 0.1	0.218 ± 0.01	64.4
Cr (VI)	mg/L	763 ± 2.6	65.7 ± 1.5	91.4

Data are represented by the mean of three replicates ± SD.

2.5. Reusability Test

The reusability test which indicates the stability of nanocatalysts is a crucial factor that should be investigated before being applied to the large scale [82]. In the current study, the reusability test of green-synthesized CuO-NPs to decolorized tanning effluent was checked under optimum conditions (at a concentration of 2 mg/mL of nanocatalyst after 200 min under sunlight irradiation conditions). Data analysis showed that the activity of nanocatalyst CuO-NPs decreased with percentages of 8.2% after five repeated cycles. As shown in Figure 9 the activity percentages of synthesized CuO-NPs to decolorize tanning wastewater was 88.2 ± 0.9% which decreased after repeating the cycles to 86.9 ± 0.5%, 85.4 ± 0.7%, 82.1 ± 0.5%, and 80.0 ± 0.3% after five cycles (Figure 9).

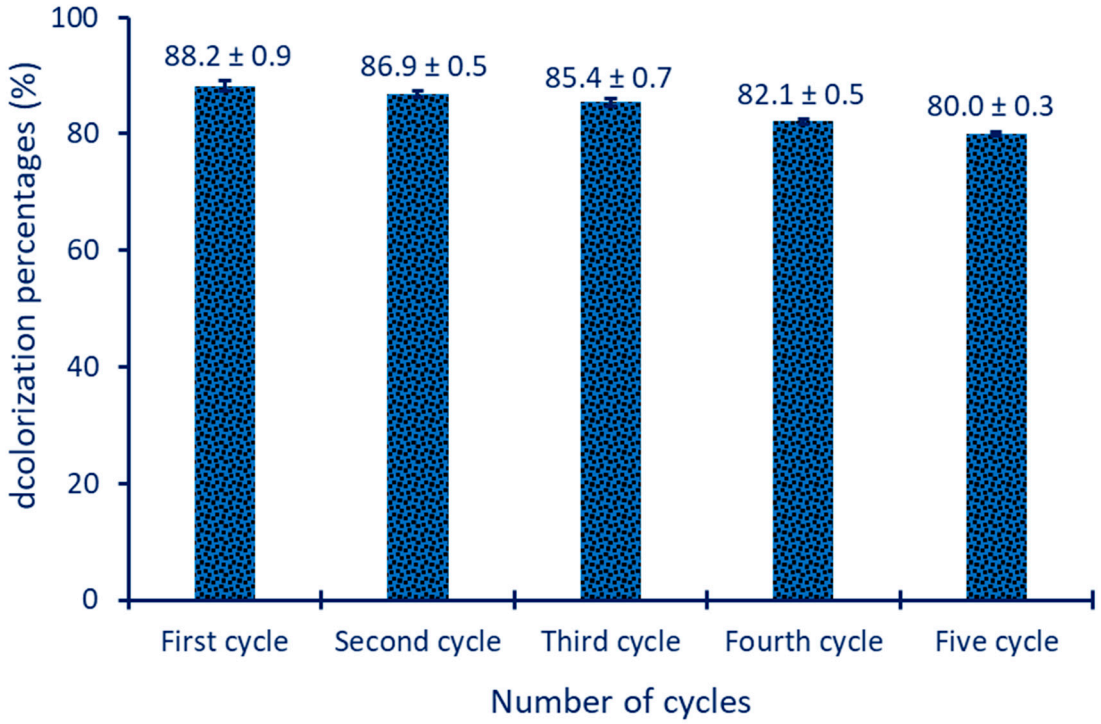

Figure 9. Reusability test for investigate the activity of green-synthesized CuO-NPs for decolorization of tanning wastewater for several cycles.

2.6. Heavy Metal Removal

Heavy metal pollution is thought to be one of the major factors to impact on humans, plants, animals, water bodies, and soils when discharged into the ecosystem without treatment. These harmful effects are due to their poisonous, non-biodegradable, and persistent characteristics. The sources of these heavy metals are either natural sources such as erosion and weathering or anthropogenic sources such as mining, car exhaust emissions, and industrialization [83–85]. Therefore, there is an urgent need to overcome this challenge using an ecofriendly and green approach. Nanomaterials provide a promising sorbent agent to remove heavy metals [19]. Tanning wastewater is considered the main and predominant source for releasing heavy metals into an ecosystem. The importance of catalysts, especially those synthesized using an eco-friendly approach, is increased when they are applied in the environment to sorption of different heavy metals. In the current study, the heavy metal content in the obtained treated tanning wastewater from optimum conditions was assessed compared to untreated samples. As shown, the crude tanning wastewater contains various heavy metals including Co, Pb, Ni, Cd, and Cr (VI) with values of 2.55 ± 0.1, 1.702 ± 0.01, 2.803 ± 0.01, 0.612 ± 0.1, and 763 ± 2.6 mg/L, respectively (Table 1). The greenish-blue color of crude tanning wastewater could be attributed to the overuse of chromium during the leather-hiding process [71]. Therefore, the maximum value of heavy metals was recorded for Cr (VI). After treatment with CuO-NPs and under optimum conditions, the values of heavy metals were decreased with percentages of 73.2, 80.8, 72.4, 64.4, and 91.4% for Co, Pb, Ni, Cd, and Cr (VI), respectively (Table 1). The high heavy metal removal using 2 mg/mL of CuO-NPs could be attributed to the availability of high adsorption sites. In the current study, the synthesized CuO-NPs have small sizes (5–30 nm), which leads to a high surface area and hence increases the adsorption sites [86]. Recently, CuO-NPs was revealed as a promising nano-sorbent for the removal of mercury and chromium ions from contaminated water with percentages of 75 and 92%, respectively [87]. In addition, green-synthesized CuO-NPs using an aqueous solution of orange peels and mint leaves displayed high activity in the removal of Pb, Ni, and Cd from contaminated water [19]. Nano-silver (Ag-NPs) and CuO-NPs fabricated using aqueous extract of *Catharanthus roseus* leaves were used to remove cadmium and chromium from a stock solution (50 ppm). The Ag-NPs showed removal efficacy with percentages of 47.8% and 5.7% for Cr and Cd, respectively, compared to removal percentages of 2.1% and 2.9% obtained using CuO-NPs [10].

Data recorded in Table 2 show some examples for green-synthesized CuO-NPs using plant extracts and their catalytic activity based on sizes and shapes. As shown, the synthesized CuO-NPs in the current study reveals various applications such as antibacterial, antifungal, wastewater treatment, and heavy metal sorption. This promising activity could be related to small sizes (5–30 nm) compared to others published research.

Table 2. Comparative study for the catalytic activity of some example for plant synthesized CuO-NPs.

Plant Precursor	Size and Shape	Applications	Testing Conditions	Catalytic Activity (Degradation Rate)	Ref.
Leaves aqueous extract of *Eucalyptus Globoulus*	88 nm, spherical	Adsorption of methyl orange dye	pH 6.5, CuO NPs dose (0.045 g/L), and dye concentration (45 mg/L).	96%	[3]
Leaves extract of mint and orange peels	150 nm, spherical	Heavy metal (Pb, Ni, and Cd) adsorption	pH 6, contact time (60 min.), CuO NPs dose (0.33 g L^{-1})	84% (Pb), 52.5% (Ni), and 18% (Cd)	[19]

Table 2. *Cont.*

Plant Precursor	Size and Shape	Applications	Testing Conditions	Catalytic Activity (Degradation Rate)	Ref.
Leaves extract of *Camellia sinensis*	6 nm, spherical	Photocatalytic degradation of methylene blue	pH 9, contact time (180 min.), CuO NPs dose (10 mg/mL), dye concentration (100 µg/mL)	85.5%	[32]
Bark extract of *Prunus africana*	8 nm, spherical	Photocatalytic degradation of methylene blue (MB)	pH 9, contact time (180 min.), CuO NPs dose (10 mg/mL), dye concentration (100 µg/mL)	83.2%	[32]
Leaves extract of *Solanum lycopersicum*	20–40 nm, spherical	Photocatalytic degradation of crystal violet	Contact time (300 min.), CuO NPs dose (25 mg), light source (visible), dye concentration (0.1 mg/100 mL).	97%	[76]
Aqueous extract of *Serratula coronata*	28 nm	Photocatalytic activity of MB	CuO NPs dose (100 mg/mL), Contact time (100 min.), light source (visible)	69%	[88]
Leave aqueous extract of *Portulaca olracea*	5–30 nm, spherical	Tanning wastewater treatment, and heavy metals (Co, Pb, Ni, Cd, and Cr) sorption	Contact time (200 min.), CuO NPs dose (2.0 mg/mL), sunlight,	Decolorization percentage was 88.6 ± 1.5%; heavy metal removal percentages of 73.2 (Co), 80.8 (Pb), 72.4 (Ni), 64.4 (Cd), and 91.4 (Cr)	Current study

3. Materials and Methods

3.1. Materials

The copper acetate, $Cu(CH_3COO)_2.H_2O$ which was used as a metal precursor for the synthesis of CuO-NPs was analytical grade and obtained from Sigma Aldrich, Egypt. The leaves of *P. oleracea* which were used for the green synthesis of CuO-NPs were collected from cultivated land in El-Menofia governorate. The bacterial strains designated as *Staphylococcus aureus*, *Bacillus subtilis*, *E. coli*, and *Pseudomonas aeruginosa* were used to investigate the antibacterial activity and purchased from American Type Culture Collection (ATCC). Tanning wastewater was collected from Robbiki Leather City, 10th of Ramadan, Cairo, Egypt (GPS: 30°17′898″N: 31°76′840″ E). All reactions were achieved using dH_2O.

3.2. Green Synthesis of CuO-NPs Using Aqueous Extract of Portulaca oleracea

The *P. oleracea* leaves were collected and washed thrice with tap water to remove any foreign debris followed by drying at 40 °C to form ash and grind to a powder. After that, 7 g of the prepared powder was mixed with 100 mL dH_2O under stirring conditions and subjected to heating at 50 °C for one hour before centrifugation at 1000 rpm for 10 min and the supernatant collected and used for biosynthesis of CuO-NPs as follows: 100 µg of $Cu(CH_3COO)_2.H_2O$ was dissolved in 90 mL dH_2O, mixed well and completed to 100 mL with plant extract which was added dropwise to derive a final concentration of 5 mM. The previous mixture was subjected to stirring for one hour and drops of 1N NaOH were added to adjust the pH to 8. The greenish precipitate was collected by centrifugation at 1000 rpm for 10 min and washed thrice with dH_2O before being heated to dry at 200 °C for four hours [52].

3.3. Characterization

The sizes and shapes of plant-based CuO-NPs were analyzed using Transmission electron microscopy (TEM, JEOL, Ltd-1010, Tokyo, Japan). The CuO-NPs powder was dispersed in water using ultra-sonification and a few drops were loaded on the TEM-carbon grid before being subjected to analysis. The particle size of synthesized CuO-NPs based on TEM image was analyzed using ImageJ software v1.52a (NIH, Bethesda, MD, USA) for more than 100 measurements from different images [89]. In addition, the qualitative and quantitative chemical composition of plant-based CuO-NPs was assessed with Energy dispersive X-ray (EDX) apparatus (JEOL, JSM-6360LA, Tokyo, Japan) through scanning electron microscopy image analysis [54]. The crystallinity structure of plant-based CuO-NPs was detected with X-ray diffraction using a PANanalytical-X'Pert-Pro-MRD equipped with CuKα as an X-ray radiation source (λ = 1.54 Å) at a current of 30 mA and voltage of 40 KV. The analysis was achieved in the range of two Theta values from 10°–80° [90]. The average crystallite size of plant-based CuO-NPs was calculated using XRD analysis using Debye–Scherrer's equation as follows [91]:

$$\text{Average crystallite size} = \frac{0.94 \times 1.54}{\beta \ \cos\theta} \quad (1)$$

where 0.94 is a Scherrer constant, 1.54 is the wavelength of the X-ray, β is the full width of the diffraction peak at a half maximum, and θ is the diffraction angle.

Fourier transform infrared (FT-IR) analysis was used to investigate the functional groups in aqueous extract and which were then compared to functional groups in plant-mediated biosynthesis of CuO-NPs. In this method, approximately 10 mg of synthesized CuO-NPs were mixed with KBr, mixed well, and subjected to pressure to form a disk that underwent scanning by FT-IR (Cary-660 model) in the ranges of 4000–400 cm^{-1} [3].

The formation of a greenish color was monitored by measuring its absorbance at a wavelength in the range of 200–800 nm using UV-Visible spectroscopy (JENWAY 6305, Staffordshire, UK). Approximately 2 mL of the synthesized solution was put in a quartz cuvette and their absorbance measured at regular time intervals to detect the maximum surface plasmon resonance (SPR).

Moreover, the hydrodynamic size as well as the size distribution in colloidal solution was detected using dynamic light scattering (DLS) (Nano-ZS, Malvern Ltd., Malvern, UK). The synthesized CuO -NPs were suspended in a highly pure solvent (MiliQ H_2O) to avoid the appearance of shadow on the signal during scattering analysis. Moreover, the surface charge of synthesized CuO-NPs was assessed using the Zetasizer apparatus (Nano-ZS, Malvern, UK).

3.4. Antimicrobial Activity

The antimicrobial activity of green-synthesized CuO-NPs was explored against different pathogenic microbes including *Bacillus subtilis* ATCC6633, *Staphylococcus aureus* ATCC6538 (Gram-positive bacteria), *Escherichia coli* ATCC8739, *Pseudomonas aeruginosa* ATCC9027 (Gram-negative bacteria), and *Candida albicans* ATCC10231 (unicellular fungi) by the agar well diffusion method [92]. The test organisms were sub-cultured on nutrient agar (for bacteria) and yeast extract peptone dextrose (YEPD) agar media (for *C. albicans*) and incubated at 35 ± 2 °C for 24 h. At the end of the incubation period, a single colony from sub-cultured organisms was picked up by sterile swap and spread uniformly over the surface of the Muller Hinton agar plate (Ready-prepared, Oxoid) before being prepared in wells (0.7 mm in diameter). Approximately, 100 µL of prepared CuO-NPs colloidal solutions (200, 100, 50, 25, 12.5, 6.25, and 3.12 µg mL^{-1}) were added to wells before being incubated at 35 ± 2 °C for 24 h. The DMSO (solvent system) was used as a control. In the end, the positive results were recorded as the diameter (mm) of clear zones formed around each well. The minimum inhibitory concentration (MIC) for each organism was detected as the lowest concentration of synthesized CuO-NPs that formed a clear zone [93]. The

experiments were performed in triplicate and the data are represented as average values and standard deviation intervals.

3.5. Tanning Wastewater Treatment

The catalytic activity of green-synthesized CuO-NPs was investigated using the degradation and decolorization of crude tanning wastewater at different concentrations (0.5, 1.0, 1.5, and 2.0 mg/mL) for various contact times (20, 40, 60, 80, 100, 120, 140, 160, 180, and 200 min) under dark and sunlight incubation conditions. The catalytic experiment was achieved at 35 ± 2 °C and measured the pH of the treatment solution before and after treatment. The catalytic batch was created under aeration condition using low-pressure, high efficiency blower and a medium bubble diffuser assembly. A known volume of tanning wastewater was mixed with a specific concentration of synthesized CuO-NPs and subjected to stirring (150 rpm) for 30 min before the experiment to attain the absorption/desorption equilibrium. One set of experiments was incubated under dark conditions and a similar set was incubated under sunlight irradiation conditions. Each treatment was achieved in triplicates. The decolorization percentages (%) were measured through the withdrawal of 1 mL of the mixture after specific times, centrifuged at 10,000 rpm for 5 min, and their absorbance measured at a wavelength of 550 nm using a spectrophotometer (721-Spectro., M-ETCAL). The percentages (%) of decolorization were calculated using the following equation [94]:

$$\text{Decolorization percentages}(\%) = \frac{A_0 - A_t}{A_0} \times 100 \quad (2)$$

where A_0 is the absorbance at 0 h (before experimenting) and A_t is the absorbance at the end of a specific time.

The physicochemical characteristics of tanning wastewater were measured from a sample obtained from optimum conditions. These characteristics including chemical oxygen demand (COD), biological oxygen demand (BOD), total dissolved solids (TDS), total suspended solids (TSS), and conductivity were measured according to standard methods [95]. Moreover, the heavy metals [lead (Pb), cobalt (Co), nickel (Ni), cadmium (Cd), and chromium (Cr)] were measured from the sample obtained from optimum conditions and compared to untreated wastewater. These heavy metals were measured using atomic adsorption spectroscopy (A PerkinElmer Analyst 800 atomic spectrometer).

3.6. Statistical Analysis

The obtained data in the current study are represented as means of three replicates ± standard deviation (±SD). The raw data were analyzed using the statistical package SPSS-V17. The difference between varied treatments was analyzed with the ANOVA (analysis of variance) test followed by Tukey's HSD test at $p < 0.05$.

4. Conclusions

- Copper oxide nanoparticles were prepared using Egyptian purslane extract as a reducing agent; such a green method is safe, easy, and cost-effective compared to the other physical and chemical methods.
- We obtained spherical, tiny (5–30 nm size range), crystalline, and highly stable (zeta-potential value of −24.6 mV) CuO-NP
- The green CuO-NP inhibited the growth of tested pathogens (*Staphylococcus aureus*, *Bacillus subtilis*, *E. coli*, *Pseudomonas aeruginosa*, and *Candida albicans*) with small concentrations (MIC range = 6.25–25 µg/mL.).
- The catalytic activity of CuO-NP in darkness recorded 70.3% decolorization, while sunlight irradiation improved the catalytic activity of nanoparticles to 88.6%.
- CuO-NP proved to be a powerful nano-sorbent, reducing Co, Pb, Ni, Cd, and Cr (VI) in wastewater with percentages of 73.2, 80.8, 72.4, 64.4, and 91.4%, respectively.

- Nano-treatment of tannery wastewater was effective in reducing the physicochemical properties of the wastewater, including TSS, TDS, COD, BOD, and conductivity with percentages of 95.2, 86.7, 91.4, 87.2, and 97.2%, respectively.
- It can be concluded that biosynthetic CuO-NPs have a dual function in the control of pathogenic microbes and the wastewater treatment of tanneries, and we recommend that they be implemented in practice.

Author Contributions: Conceptualization, A.M.E., A.F., and S.E.-D.H.; methodology, A.M.E., A.F., S.E.-D.H., M.F.H., and W.M.S.; software, A.M.E., A.F., S.E.-D.H., M.F.H., and W.M.S.; validation, A.M.E., A.F., S.E.-D.H., M.F.H., N.K.A., A.E., A.A., and W.M.S.; formal analysis, A.M.E., A.F., S.E.-D.H., M.F.H., N.K.A., A.E., A.A., and W.M.S.; investigation, A.M.E., A.F., S.E.-D.H., M.F.H., and W.M.S.; resources, A.M.E., A.F., S.E.-D.H., M.F.H., N.K.A., A.E., A.A., and W.M.S.; data curation, A.M.E., A.F., S.E.-D.H., M.F.H., N.K.A., A.E., A.A., and W.M.S.; writing—original draft preparation, A.M.E., A.F.; writing—review and editing, A.M.E., A.F., S.E.-D.H., M.F.H., and W.M.S.; visualization, A.M.E., A.F., S.E.-D.H., M.F.H., N.K.A., A.E., A.A., and W.M.S.; supervision, A.M.E., A.F., and S.E.-D.H.; project administration, A.M.E., A.F., and S.E.-D.H.; funding acquisition, A.M.E., A.F., S.E.-D.H., M.F.H., N.K.A., A.E., A.A., and W.M.S. All authors have read and agreed to the published version of the manuscript.

Funding: This research received no external funding.

Data Availability Statement: The data presented in this study are available on request from the corresponding author.

Acknowledgments: We want to acknowledge Princess Nourah bint Abdulrahman University Researchers Supporting Project number (PNURSP2023R153), Princess Nourah bint Abdulrahman University, Riyadh, Saudi Arabia.

Conflicts of Interest: The authors declare no conflict of interest.

References

1. Urban-Chmiel, R.; Marek, A.; Stępień-Pyśniak, D.; Wieczorek, K.; Dec, M.; Nowaczek, A.; Osek, J. Antibiotic Resistance in Bacteria-A Review. *Antibiotics* **2022**, *11*, 1079. [CrossRef] [PubMed]
2. Hamza, M.F.; Guibal, E.; Wei, Y.; Fouda, A. Magnetic Amino-Sulfonic Dual Sorbent for Uranyl Sorption from Aqueous Soultions–Influence of Light Irradiation on Sorption Properties. *Chem. Eng. J.* **2023**, *456*, 141099. [CrossRef]
3. Alhalili, Z. Green synthesis of copper oxide nanoparticles CuO NPs from *Eucalyptus globoulus* leaf extract: Adsorption and design of experiments. *Arab. J. Chem.* **2022**, *15*, 103739. [CrossRef]
4. Fouda, A.; Al-Otaibi, W.A.; Saber, T.; AlMotwaa, S.M.; Alshallash, K.S.; Elhady, M.; Badr, N.F.; Abdel-Rahman, M.A. Antimicrobial, Antiviral, and In-Vitro Cytotoxicity and Mosquitocidal Activities of *Portulaca oleracea*-Based Green Synthesis of Selenium Nanoparticles. *J. Funct. Biomater.* **2022**, *13*, 157. [CrossRef] [PubMed]
5. Hamza, M.F.; Abdel-Rahman, A.A.H.; Hawata, M.A.; El Araby, R.; Guibal, E.; Fouda, A.; Wei, Y.; Hamad, N.A. Functionalization of magnetic chitosan microparticles—Comparison of trione and trithione grafting for enhanced silver sorption and application to metal recovery from waste X-ray photographic films. *J. Environ. Chem. Eng.* **2022**, *10*, 107939. [CrossRef]
6. Fouda, A.; Hassan, S.E.-D.; Eid, A.M.; Abdel-Rahman, M.A.; Hamza, M.F. Light enhanced the antimicrobial, anticancer, and catalytic activities of selenium nanoparticles fabricated by endophytic fungal strain, *Penicillium crustosum* EP-1. *Sci. Rep.* **2022**, *12*, 11834. [CrossRef]
7. Hamza, M.F.; Guibal, E.; Abdel-Rahman, A.A.-H.; Salem, M.; Khalafalla, M.S.; Wei, Y.; Yin, X. Enhancement of Cerium Sorption onto Urea-Functionalized Magnetite Chitosan Microparticles by Sorbent Sulfonation—Application to Ore Leachate. *Molecules* **2022**, *27*, 7562. [CrossRef]
8. Bhavyasree, P.G.; Xavier, T.S. Green synthesised copper and copper oxide based nanomaterials using plant extracts and their application in antimicrobial activity: Review. *Curr. Res. Green Sustain. Chem.* **2022**, *5*, 100249. [CrossRef]
9. Bhavyasree, P.G.; Xavier, T.S. Adsorption studies of Methylene Blue, Coomassie Brilliant Blue, and Congo Red dyes onto CuO/C nanocomposites synthesized via *Vitex negundo* Linn leaf extract. *Curr. Res. Green Sustain. Chem.* **2021**, *4*, 100161. [CrossRef]
10. Verma, A.; Bharadvaja, N. Plant-Mediated Synthesis and Characterization of Silver and Copper Oxide Nanoparticles: Antibacterial and Heavy Metal Removal Activity. *J. Clust. Sci.* **2022**, *33*, 1697–1712. [CrossRef]
11. Zhou, Y.-X.; Xin, H.-L.; Rahman, K.; Wang, S.-J.; Peng, C.; Zhang, H. *Portulaca oleracea* L.: A Review of Phytochemistry and Pharmacological Effects. *BioMed Res. Int.* **2015**, *2015*, 925631. [CrossRef] [PubMed]
12. Al-Otibi, F.; Alfuzan, S.A.; Alharbi, R.I.; Al-Askar, A.A.; Al-Otaibi, R.M.; Al Subaie, H.F.; Moubayed, N.M.S. Comparative study of antifungal activity of two preparations of green silver nanoparticles from *Portulaca oleracea* extract. *Saudi J. Biol. Sci.* **2022**, *29*, 2772–2781. [CrossRef] [PubMed]

13. Al-Sagheer, L.A.M.; Elsayed, W.; Al-Ghamdi, A.A.; Alshehrie, A. Light interaction with the copper nanocrystals with various sizes prepared via *portulaca oleracea* assisted polyol technique. *Optik* **2020**, *203*, 163901. [CrossRef]
14. Ouidad, A.; Sara, C.; Samir, D. Biological properties and Acute Toxicity Study of Copper oxide nanoparticles prepared by aqueous leaves extract of *Portulaca oleracea* (L). *Asian J. Pharm. Res.* **2020**, *10*, 89–94. [CrossRef]
15. Epelle, E.I.; Okoye, P.U.; Roddy, S.; Gunes, B.; Okolie, J.A. Advances in the Applications of Nanomaterials for Wastewater Treatment. *Environments* **2022**, *9*, 141. [CrossRef]
16. Zhao, J.; Wu, Q.; Tang, Y.; Zhou, J.; Guo, H. Tannery wastewater treatment: Conventional and promising processes, an updated 20-year review. *J. Leather Sci. Eng.* **2022**, *4*, 10. [CrossRef]
17. Singh, S.; Kumar, V.; Romero, R.; Sharma, K.; Singh, J. Applications of Nanoparticles in Wastewater Treatment. In *Nanobiotechnology in Bioformulations*; Prasad, R., Kumar, V., Kumar, M., Choudhary, D., Eds.; Springer International Publishing: Cham, Gemany, 2019; pp. 395–418.
18. Darwesh, O.M.; Li, H.; Matter, I.A. Nano-bioremediation of textile industry wastewater using immobilized CuO-NPs myco-synthesized by a novel Cu-resistant *Fusarium oxysporum* OSF18. *Environ. Sci. Pollut. Res.* **2022**. [CrossRef]
19. Mahmoud, A.E.D.; Al-Qahtani, K.M.; Alflaij, S.O.; Al-Qahtani, S.F.; Alsamhan, F.A. Green copper oxide nanoparticles for lead, nickel, and cadmium removal from contaminated water. *Sci. Rep.* **2021**, *11*, 12547. [CrossRef]
20. Saied, E.; Eid, A.M.; Hassan, S.E.; Salem, S.S.; Radwan, A.A.; Halawa, M.; Saleh, F.M.; Saad, H.A.; Saied, E.M.; Fouda, A. The Catalytic Activity of Biosynthesized Magnesium Oxide Nanoparticles (MgO-NPs) for Inhibiting the Growth of Pathogenic Microbes, Tanning Effluent Treatment, and Chromium Ion Removal. *Catalysts* **2021**, *11*, 821. [CrossRef]
21. Bouafia, A.; Laouini, S.E.; Tedjani, M.L.; Ali, G.A.M.; Barhoum, A. Green biosynthesis and physicochemical characterization of Fe_3O_4 nanoparticles using *Punica granatum* L. fruit peel extract for optoelectronic applications. *Text. Res. J.* **2021**, *92*, 2685–2696. [CrossRef]
22. Salem, S.S.; Fouda, A. Green Synthesis of Metallic Nanoparticles and Their Prospective Biotechnological Applications: An Overview. *Biol. Trace Elem. Res.* **2021**, *199*, 344–370. [CrossRef]
23. Chand Mali, S.; Raj, S.; Trivedi, R. Biosynthesis of copper oxide nanoparticles using *Enicostemma axillare* (Lam.) leaf extract. *Biochem. Biophys. Rep.* **2019**, *20*, 100699. [CrossRef] [PubMed]
24. Ghaffar, N.; Javad, S.; Farrukh, M.A.; Shah, A.A.; Gatasheh, M.K.; Al-Munqedhi, B.M.; Chaudhry, O. Metal nanoparticles assisted revival of Streptomycin against MDRS *Staphylococcus aureus*. *PLoS ONE* **2022**, *17*, e0264588. [CrossRef] [PubMed]
25. Mahmood, R.I.; Kadhim, A.A.; Ibraheem, S.; Albukhaty, S.; Mohammed-Salih, H.S.; Abbas, R.H.; Jabir, M.S.; Mohammed, M.K.A.; Nayef, U.M.; AlMalki, F.A.; et al. Biosynthesis of copper oxide nanoparticles mediated *Annona muricata* as cytotoxic and apoptosis inducer factor in breast cancer cell lines. *Sci. Rep.* **2022**, *12*, 16165. [CrossRef]
26. Tabrez, S.; Khan, A.U.; Mirza, A.A.; Suhail, M.; Jabir, N.R.; Zughaibi, T.A.; Alam, M. Biosynthesis of copper oxide nanoparticles and its therapeutic efficacy against colon cancer. *Nanotechnol. Rev.* **2022**, *11*, 1322–1331. [CrossRef]
27. Wongrakpanich, A.; Mudunkotuwa, I.A.; Geary, S.M.; Morris, A.S.; Mapuskar, K.A.; Spitz, D.R.; Grassian, V.H.; Salem, A.K. Size-dependent cytotoxicity of copper oxide nanoparticles in lung epithelial cells. *Environ. Science. Nano* **2016**, *3*, 365–374. [CrossRef] [PubMed]
28. Tavakoli, S.; Kharaziha, M.; Ahmadi, S. Green synthesis and morphology dependent antibacterial activity of copper oxide nanoparticles. *J. Nanostruct.* **2019**, *9*, 163–171.
29. Gao, P.; Liu, D. Facile synthesis of copper oxide nanostructures and their application in non-enzymatic hydrogen peroxide sensing. *Sens. Actuators B Chem.* **2015**, *208*, 346–354. [CrossRef]
30. Al-Qasmi, N. Facial Eco-Friendly Synthesis of Copper Oxide Nanoparticles Using Chia Seeds Extract and Evaluation of Its Electrochemical Activity. *Processes* **2021**, *9*, 2027. [CrossRef]
31. Anwaar, S.; Maqbool, Q.; Jabeen, N.; Nazar, M.; Abbas, F.; Nawaz, B.; Hussain, T.; Hussain, S.Z. The Effect of Green Synthesized CuO Nanoparticles on Callogenesis and Regeneration of *Oryza sativa* L. *Front. Plant Sci.* **2016**, *7*, 1330. [CrossRef]
32. Ssekatawa, K.; Byarugaba, D.K.; Angwe, M.K.; Wampande, E.M.; Ejobi, F.; Nxumalo, E.; Maaza, M.; Sackey, J.; Kirabira, J.B. Phyto-Mediated Copper Oxide Nanoparticles for Antibacterial, Antioxidant and Photocatalytic Performances. *Front. Bioeng. Biotechnol.* **2022**, *10*, 820218. [CrossRef] [PubMed]
33. Rehman, S.; Mumtaz, A.; Hasanain, S.K. Size effects on the magnetic and optical properties of CuO nanoparticles. *J. Nanopart. Res.* **2011**, *13*, 2497–2507. [CrossRef]
34. Naz, S.; Gul, A.; Zia, M. Toxicity of copper oxide nanoparticles: A review study. *IET Nanobiotechnol.* **2020**, *14*, 1–13. [CrossRef]
35. Fouda, A.; Salem, S.S.; Wassel, A.R.; Hamza, M.F.; Shaheen, T.I. Optimization of green biosynthesized visible light active CuO/ZnO nano-photocatalysts for the degradation of organic methylene blue dye. *Heliyon* **2020**, *6*, e04896. [CrossRef]
36. Ahamed, M.; Alhadlaq, H.A.; Khan, M.A.M.; Karuppiah, P.; Al-Dhabi, N.A. Synthesis, Characterization, and Antimicrobial Activity of Copper Oxide Nanoparticles. *J. Nanomater.* **2014**, *2014*, 637858. [CrossRef]
37. Karthik, C.; Suresh, S.; Sneha Mirulalini, G.; Kavitha, S. A FTIR approach of green synthesized silver nanoparticles by *Ocimum sanctum* and *Ocimum gratissimum* on mung bean seeds. *Inorg. Nano-Met. Chem.* **2020**, *50*, 606–612.
38. Hamza, M.F.; Hamad, D.M.; Hamad, N.A.; Abdel-Rahman, A.A.H.; Fouda, A.; Wei, Y.; Guibal, E.; El-Etrawy, A.-A.S. Functionalization of magnetic chitosan microparticles for high-performance removal of chromate from aqueous solutions and tannery effluent. *Chem. Eng. J.* **2022**, *428*, 131775. [CrossRef]

39. Zaaeri, F.; Khoobi, M.; Rouini, M.; Akbari Javar, H. pH-responsive polymer in a core–shell magnetic structure as an efficient carrier for delivery of doxorubicin to tumor cells. *Int. J. Polym. Mater. Polym. Biomater.* **2018**, *67*, 967–977. [CrossRef]
40. Khademi-Azandehi, P.; Moghaddam, J. Green synthesis, characterization and physiological stability of gold nanoparticles from *Stachys lavandulifolia* Vahl extract. *Particuology* **2015**, *19*, 22–26. [CrossRef]
41. Coates, J. Interpretation of Infrared Spectra, A Practical Approach. In *Encyclopedia of Analytical Chemistry, Applications, Theory, and Instrumentation*; Sons, J.W., Ed.; John Wiley & Sons, Inc.: Hoboken, NJ, USA, 2000.
42. Zahra, M.H.; Hamza, M.F.; El-Habibi, G.; Abdel-Rahman, A.A.H.; Mira, H.I.; Wei, Y.; Alotaibi, S.H.; Amer, H.H.; Goda, A.E.S.; Hamad, N.A. Synthesis of a Novel Adsorbent Based on Chitosan Magnetite Nanoparticles for the High Sorption of Cr (VI) Ions: A Study of Photocatalysis and Recovery on Tannery Effluents. *Catalysts* **2022**, *12*, 678. [CrossRef]
43. Fouda, A.; Eid, A.M.; Abdel-Rahman, M.A.; EL-Belely, E.F.; Awad, M.A.; Hassan, S.E.-D.; AL-Faifi, Z.E.; Hamza, M.F. Enhanced Antimicrobial, Cytotoxicity, Larvicidal, and Repellence Activities of Brown Algae, *Cystoseira crinita*-Mediated Green Synthesis of Magnesium Oxide Nanoparticles. *Front. Bioeng. Biotechnol.* **2022**, *10*, 849921. [CrossRef]
44. Hamza, M.F.; Abu Khoziem, H.A.; Khalafalla, M.S.; Abdellah, W.M.; Zaki, D.I.; Althumayri, K.; Wei, Y. Ecofriendly Composite as a Promising Material for Highly-Performance Uranium Recovery from Different Solutions. *Toxics* **2022**, *10*, 490. [CrossRef]
45. Saha, N.; Trivedi, P.; Dutta Gupta, S. Surface Plasmon Resonance (SPR) Based Optimization of Biosynthesis of Silver Nanoparticles from Rhizome Extract of *Curculigo orchioides* Gaertn. and Its Antioxidant Potential. *J. Clust. Sci.* **2016**, *27*, 1893–1912. [CrossRef]
46. Sakugawa, K.; Ikeda, A.; Takemura, A.; Ono, H. Simplified method for estimation of composition of alginates by FTIR. *J. Appl. Polym. Sci.* **2004**, *93*, 1372–1377. [CrossRef]
47. Hamza, M.F.; Salih, K.A.M.; Abdel-Rahman, A.A.H.; Zayed, Y.E.; Wei, Y.; Liang, J.; Guibal, E. Sulfonic-functionalized algal/PEI beads for scandium, cerium and holmium sorption from aqueous solutions (synthetic and industrial samples). *Chem. Eng. J.* **2021**, *403*, 126399. [CrossRef]
48. Lawrie, G.; Keen, I.; Drew, B.; Chandler-Temple, A.; Rintoul, L.; Fredericks, P.; Grøndahl, L. Interactions between Alginate and Chitosan Biopolymers Characterized Using FTIR and XPS. *Biomacromolecules* **2007**, *8*, 2533–2541. [CrossRef] [PubMed]
49. Hamza, M.F.; Guibal, E.; Althumayri, K.; Wei, Y.; Eid, A.M.; Fouda, A. Poly-condensation of N-(2-acetamido)-2-aminoethanesulfonic acid with formaldehyde for the synthesis of a highly efficient sorbent for Cs(I). *Chem. Eng. J.* **2023**, *454*, 140155. [CrossRef]
50. Dangi, Y.R.; Bediako, J.K.; Lin, X.; Choi, J.-W.; Lim, C.-R.; Song, M.-H.; Han, M.; Yun, Y.-S. Polyethyleneimine impregnated alginate capsule as a high capacity sorbent for the recovery of monovalent and trivalent gold. *Sci. Rep.* **2021**, *11*, 17836. [CrossRef]
51. Fouda, A.; Eid, A.M.; Abdelkareem, A.; Said, H.A.; El-Belely, E.F.; Alkhalifah, D.H.M.; Alshallash, K.S.; Hassan, S.E. Phyco-Synthesized Zinc Oxide Nanoparticles Using Marine Macroalgae, *Ulva fasciata* Delile, Characterization, Antibacterial Activity, Photocatalysis, and Tanning Wastewater Treatment. *Catalysts* **2022**, *12*, 756. [CrossRef]
52. Djamila, B.; Eddine, L.S.; Abderrhmane, B.; Nassiba, A.; Barhoum, A. In vitro antioxidant activities of copper mixed oxide (CuO/Cu_2O) nanoparticles produced from the leaves of *Phoenix dactylifera* L. *Biomass Convers. Biorefinery* **2022**. [CrossRef]
53. Yang, Y.; Xu, D.; Wu, Q.; Diao, P. Cu_2O/CuO Bilayered Composite as a High-Efficiency Photocathode for Photoelectrochemical Hydrogen Evolution Reaction. *Sci. Rep.* **2016**, *6*, 35158. [CrossRef] [PubMed]
54. Fouda, A.; Hassan, S.E.-D.; Eid, A.M.; Awad, M.A.; Althumayri, K.; Badr, N.F.; Hamza, M.F. Endophytic bacterial strain, *Brevibacillus brevis*-mediated green synthesis of copper oxide nanoparticles, characterization, antifungal, in vitro cytotoxicity, and larvicidal activity. *Green Process. Synth.* **2022**, *11*, 931–950. [CrossRef]
55. Fouda, A.; Eid, A.M.; Guibal, E.; Hamza, M.F.; Hassan, S.E.; Alkhalifah, D.H.M.; El-Hossary, D. Green Synthesis of Gold Nanoparticles by Aqueous Extract of *Zingiber officinale*: Characterization and Insight into Antimicrobial, Antioxidant, and In Vitro Cytotoxic Activities. *Appl. Sci.* **2022**, *12*, 12879. [CrossRef]
56. Tomaszewska, E.; Soliwoda, K.; Kadziola, K.; Tkacz-Szczesna, B.; Celichowski, G.; Cichomski, M.; Szmaja, W.; Grobelny, J. Detection Limits of DLS and UV-Vis Spectroscopy in Characterization of Polydisperse Nanoparticles Colloids. *J. Nanomater.* **2013**, *2013*, 313081. [CrossRef]
57. Danaei, M.; Dehghankhold, M.; Ataei, S.; Hasanzadeh Davarani, F.; Javanmard, R.; Dokhani, A.; Khorasani, S.; Mozafari, M.R. Impact of Particle Size and Polydispersity Index on the Clinical Applications of Lipidic Nanocarrier Systems. *Pharmaceutics* **2018**, *10*, 57. [CrossRef] [PubMed]
58. Bhattacharjee, S. DLS and zeta potential—What they are and what they are not? *J. Control. Release* **2016**, *235*, 337–351. [CrossRef]
59. Ibrahim, A.G.; Fouda, A.; Elgammal, W.E.; Eid, A.M.; Elsenety, M.M.; Mohamed, A.E.; Hassan, S.M. New thiadiazole modified chitosan derivative to control the growth of human pathogenic microbes and cancer cell lines. *Sci. Rep.* **2022**, *12*, 21423. [CrossRef]
60. Fouda, A.; Awad, M.A.; Eid, A.M.; Saied, E.; Barghoth, M.G.; Hamza, M.F.; Awad, M.F.; Abdelbary, S.; Hassan, S.E. An Eco-Friendly Approach to the Control of Pathogenic Microbes and *Anopheles stephensi* Malarial Vector Using Magnesium Oxide Nanoparticles (Mg-NPs) Fabricated by *Penicillium chrysogenum*. *Int. J. Mol. Sci.* **2021**, *22*, 5096. [CrossRef]
61. Qamar, H.; Rehman, S.; Chauhan, D.K.; Tiwari, A.K.; Upmanyu, V. Green synthesis, characterization and antimicrobial activity of copper oxide nanomaterial derived from *Momordica charantia*. *Int. J. Nanomed.* **2020**, *15*, 2541. [CrossRef]
62. Emerging, S.C.o.; Risks, N.I.H. *Opinion on the Appropriateness of the Risk Assessment Methodology in Accordance with the Technical Guidance Documents for New and Existing Substances for Assessing the Risks of Nanomaterials [Internet]*; European Commission Brussels: Brussels, Belgium, 2007.
63. Krithiga, N.; Jayachitra, A.; Rajalakshmi, A. Synthesis, characterization and analysis of the effect of copper oxide nanoparticles in biological systems. *Ind. J. Ns* **2013**, *1*, 6–15.

64. Hassan, S.E.; Fouda, A.; Radwan, A.A.; Salem, S.S.; Barghoth, M.G.; Awad, M.A.; Abdo, A.M.; El-Gamal, M.S. Endophytic actinomycetes *Streptomyces* spp mediated biosynthesis of copper oxide nanoparticles as a promising tool for biotechnological applications. *J. Biol. Inorg. Chem. JBIC A Publ. Soc. Biol. Inorg. Chem.* **2019**, *24*, 377–393. [CrossRef] [PubMed]
65. Abdel-Maksoud, G.; Gaballah, S.; Youssef, A.M.; Eid, A.M.; Sultan, M.H.; Fouda, A. Eco-friendly approach for control of fungal deterioration of archaeological skeleton dated back to the Greco-Roman period. *J. Cult. Herit.* **2023**, *59*, 38–48. [CrossRef]
66. Alsharif, S.M.; Salem, S.S.; Abdel-Rahman, M.A.; Fouda, A.; Eid, A.M.; El-Din Hassan, S.; Awad, M.A.; Mohamed, A.A. Multifunctional properties of spherical silver nanoparticles fabricated by different microbial taxa. *Heliyon* **2020**, *6*, e03943. [CrossRef] [PubMed]
67. Hamza, M.F.; Fouda, A.; Elwakeel, K.Z.; Wei, Y.; Guibal, E.; Hamad, N.A. Phosphorylation of Guar Gum/Magnetite/Chitosan Nanocomposites for Uranium (VI) Sorption and Antibacterial Applications. *Molecules* **2021**, *26*, 1920. [CrossRef] [PubMed]
68. Lemire, J.A.; Harrison, J.J.; Turner, R.J. Antimicrobial activity of metals: Mechanisms, molecular targets and applications. *Nat. Rev. Microbiol.* **2013**, *11*, 371–384. [CrossRef] [PubMed]
69. Warnes, S.L.; Caves, V.; Keevil, C.W. Mechanism of copper surface toxicity in *Escherichia coli* O157:H7 and *Salmonella* involves immediate membrane depolarization followed by slower rate of DNA destruction which differs from that observed for Gram-positive bacteria. *Environ. Microbiol.* **2012**, *14*, 1730–1743. [CrossRef]
70. Mohamed, A.E.; Elgammal, W.E.; Eid, A.M.; Dawaba, A.M.; Ibrahim, A.G.; Fouda, A.; Hassan, S.M. Synthesis and characterization of new functionalized chitosan and its antimicrobial and in-vitro release behavior from topical gel. *Int. J. Biol. Macromol.* **2022**, *207*, 242–253. [CrossRef]
71. Hamza, M.F.; Guibal, E.; Althumayri, K.; Vincent, T.; Yin, X.; Wei, Y.; Li, W. New Process for the Sulfonation of Algal/PEI Biosorbent for Enhancing Sr(II) Removal from Aqueous Solutions—Application to Seawater. *Molecules* **2022**, *27*, 7128. [CrossRef]
72. Fouda, A.; Hassan, S.E.-D.; Saied, E.; Hamza, M.F. Photocatalytic degradation of real textile and tannery effluent using biosynthesized magnesium oxide nanoparticles (MgO-NPs), heavy metal adsorption, phytotoxicity, and antimicrobial activity. *J. Environ. Chem. Eng.* **2021**, *9*, 105346. [CrossRef]
73. Fouda, A.; Awad, M.A.; Al-Faifi, Z.E.; Gad, M.E.; Al-Khalaf, A.A.; Yahya, R.; Hamza, M.F. *Aspergillus flavus*-Mediated Green Synthesis of Silver Nanoparticles and Evaluation of Their Antibacterial, Anti-Candida, Acaricides, and Photocatalytic Activities. *Catalysts* **2022**, *12*, 462. [CrossRef]
74. Fouda, A.; Hassan, S.E.-D.; Saied, E.; Azab, M.S. An eco-friendly approach to textile and tannery wastewater treatment using maghemite nanoparticles (γ-Fe_2O_3-NPs) fabricated by *Penicillium expansum* strain (K-w). *J. Environ. Chem. Eng.* **2021**, *9*, 104693. [CrossRef]
75. Li, S. Combustion synthesis of porous MgO and its adsorption properties. *Int. J. Ind. Chem.* **2019**, *10*, 89–96. [CrossRef]
76. Vaidehi, D.; Bhuvaneshwari, V.; Bharathi, D.; Sheetal, B.P. Antibacterial and photocatalytic activity of copper oxide nanoparticles synthesized using *Solanum lycopersicum* leaf extract. *Mater. Res. Express* **2018**, *5*, 085403. [CrossRef]
77. Deghles, A.; Kurt, U. Treatment of tannery wastewater by a hybrid electrocoagulation/electrodialysis process. *Chem. Eng. Process. Process Intensif.* **2016**, *104*, 43–50. [CrossRef]
78. Amanial, H.R. Physico-chemical characterization of tannery effluent and its impact on the nearby river. *J. Environ. Chem. Ecotoxicol.* **2016**, *8*, 44–50. [CrossRef]
79. Lkhagvadulam, B.; Tsagaantsetseg, B.; Tergel, D.; Chuluunkhuyag, S. Removal of chromium from a tannery wastewater by using a maghemite nanoparticles. *Int. J. Environ. Sci. Dev.* **2017**, *8*, 696–702. [CrossRef]
80. Zhang, D.; Trzcinski, A.P.; Oh, H.-S.; Chew, E.; Tan, S.K.; Ng, W.J.; Liu, Y. Comparison and distribution of copper oxide nanoparticles and copper ions in activated sludge reactors. *J. Environ. Sci. Health Part A* **2017**, *52*, 507–514. [CrossRef]
81. Wang, S.; Li, Z.; Gao, M.; She, Z.; Ma, B.; Guo, L.; Zheng, D.; Zhao, Y.; Jin, C.; Wang, X.; et al. Long-term effects of cupric oxide nanoparticles (CuO NPs) on the performance, microbial community and enzymatic activity of activated sludge in a sequencing batch reactor. *J. Environ. Manag.* **2017**, *187*, 330–339. [CrossRef]
82. Elfeky, A.S.; Salem, S.S.; Elzaref, A.S.; Owda, M.E.; Eladawy, H.A.; Saeed, A.M.; Awad, M.A.; Abou-Zeid, R.E.; Fouda, A. Multifunctional cellulose nanocrystal /metal oxide hybrid, photo-degradation, antibacterial and larvicidal activities. *Carbohydr. Polym.* **2020**, *230*, 115711. [CrossRef]
83. El Din Mahmoud, A.; Fawzy, M. Bio-based Methods for Wastewater Treatment: Green Sorbents. In *Phytoremediation: Management of Environmental Contaminants*; Ansari, A.A., Gill, S.S., Gill, R., Lanza, G.R., Newman, L., Eds.; Springer International Publishing: Cham, Germany, 2016; Volume 3, pp. 209–238.
84. Hamza, M.F.; Wei, Y.; Althumayri, K.; Fouda, A.; Hamad, N.A. Synthesis and Characterization of Functionalized Chitosan Nanoparticles with Pyrimidine Derivative for Enhancing Ion Sorption and Application for Removal of Contaminants. *Materials* **2022**, *15*, 4676. [CrossRef]
85. Hamza, M.F.; Alotaibi, S.H.; Wei, Y.; Mashaal, N.M. High-Performance Hydrogel Based on Modified Chitosan for Removal of Heavy Metal Ions in Borehole: A Case Study from the Bahariya Oasis. *Egypt. Catal.* **2022**, *12*, 721. [CrossRef]
86. Saeed, A.; Sharif, M.; Iqbal, M. Application potential of grapefruit peel as dye sorbent: Kinetics, equilibrium and mechanism of crystal violet adsorption. *J. Hazard. Mater.* **2010**, *179*, 564–572. [CrossRef] [PubMed]
87. Raul, P.K.; Das, B.; Umlong, I.M.; Devi, R.R.; Tiwari, G.; Kamboj, D.V. Toward a Feasible Solution for Removing Toxic Mercury and Chromium From Water Using Copper Oxide Nanoparticles. *Front. Nanotechnol.* **2022**, *4*, 2. [CrossRef]

88. Mashentseva, A.A.; Aimanova, N.A.; Temirgaziev, B.S.; Zhumazhanova, A.; Tuleuov, B.I. Photocatalytic Activity of Copper(II) Oxide Nanoparticles Synthesized Using *Serratula Coronata* L. Extract. *Pet. Chem.* **2020**, *60*, 1141–1147. [CrossRef]
89. Schindelin, J.; Arganda-Carreras, I.; Frise, E.; Kaynig, V.; Longair, M.; Pietzsch, T.; Preibisch, S.; Rueden, C.; Saalfeld, S.; Schmid, B.; et al. Fiji: An open-source platform for biological-image analysis. *Nat. Methods* **2012**, *9*, 676–682. [CrossRef] [PubMed]
90. Fouda, A.; Abdel-Nasser, M.; Khalil, A.M.A.; Hassan, S.E.-D.; Abdel-Maksoud, G. Investigate the role of fungal communities associated with a historical manuscript from the 17th century in biodegradation. *Npj Mater. Degrad.* **2022**, *6*, 88. [CrossRef]
91. Bokuniaeva, A.O.; Vorokh, A.S. Estimation of particle size using the Debye equation and the Scherrer formula for polyphasic TiO₂ powder. *J. Phys. Conf. Ser.* **2019**, *1410*, 012057.
92. Humphries, R.M.; Ambler, J.; Mitchell, S.L.; Castanheira, M.; Dingle, T.; Hindler, J.A.; Koeth, L.; Sei, K.; Standardization, C.M.D. CLSI methods development and standardization working group best practices for evaluation of antimicrobial susceptibility tests. *J. Clin. Microbiol.* **2018**, *56*, e01934-17. [CrossRef]
93. Gonelimali, F.D.; Lin, J.; Miao, W.; Xuan, J.; Charles, F.; Chen, M.; Hatab, S.R. Antimicrobial Properties and Mechanism of Action of Some Plant Extracts Against Food Pathogens and Spoilage Microorganisms. *Front. Microbiol.* **2018**, *9*, 1639. [CrossRef]
94. Fouda, A.; Hassan, S.E.-D.; Abdel-Rahman, M.A.; Farag, M.M.S.; Shehal-deen, A.; Mohamed, A.A.; Alsharif, S.M.; Saied, E.; Moghanim, S.A.; Azab, M.S. Catalytic degradation of wastewater from the textile and tannery industries by green synthesized hematite (α-Fe_2O_3) and magnesium oxide (MgO) nanoparticles. *Curr. Res. Biotechnol.* **2021**, *3*, 29–41. [CrossRef]
95. Rice, E.W.; Baird, R.B.; Eaton, A.D.; Clesceri, L.S. *Standard Methods for the Examination of Water and Wastewater*; American Public Health Association: Washington, DC, USA, 2012; Volume 10.